NOAA OAR Special Report

PMEL Tsunami Forecast Series: Vol. NNNN
Development of a Tsunami Forecast Model for Arena Cove, California

Michael C. Spillane [1,2]

[1]Joint Institute for the Study of the Atmosphere and Ocean (JISAO), University of Washington, Seattle, WA
[2]NOAA/Pacific Marine Environmental Laboratory (PMEL), Seattle, WA

April 2011

DRAFT

NOTICE from NOAA

Mention of a commercial company or product does not constitute an endorsement by NOAA/OAR. Use of information from this publication concerning proprietary products or the tests of such products for publicity or advertising purposes is not authorized. Any opinions, findings, and conclusions or recommendations expressed in this material are those of the authors and do not necessarily reflect the views of the National Oceanic and Atmospheric Administration.

Contribution No. XXXX from NOAA/Pacific Marine Environmental Laboratory

Also available from the National Technical Information Service (NTIS)
(http://www.ntis.gov)

DRAFT

Contents

List of Figures

List of Tables

Foreword

Abstract

1.0 Background and Objectives
- 1.1 The Setting
- 1.2 Natural Hazards
- 1.3 Tsunami Warning and Risk Assessment

2.0 Forecast Methodology
- 2.1 The Tsunami Model
- 2.2 The SIFT Forecast System

3.0 Model Development
- 3.1 Digital Elevation Models
- 3.2 Tides and Sea Level Variation
- 3.3 The CFL Condition and other considerations for grid design
- 3.4 Specifics of the model grids
- 3.5 Model Run Input and Output Files

4.0 Results and Discussion
- 4.1 The "Null" Tests
- 4.2 The Extreme Case Tests
- 4.3 Model Validation with Historical Events
- 4.4 Further Historical Simulations
- 4.5 The Mendocino Earthquake of April 25, 1992
- 4.6 The Honshu Tsunami of March 11, 2011
- 4.7 Simulation of further Extreme Events

5.0 Conclusions

6.0 Acknowledgements

7.0 References

FIGURES

Appendix A
- A1. Reference Model Input (*.in) File for Arena Cove, CA
- A2. Forecast Model Input (*.in) File for Arena Cove, CA

DRAFT

Appendix B Propagation Database: Pacific Ocean Unit Sources

Appendix C Synthetic Testing Report

Glossary

DRAFT

List of Figures

Figure 1. The Point Arena area of southern Mendocino County, CA.
Figure 2. Views of present-day Arena Cove and its appearance in the early 1900's.
Figure 3. Extract from the oblique 3-D view of the Arena Cove DEM, provided by NGDC; sites of potential inundation identified by CalEMA are highlighted in red.
Figure 4. Distribution of the historical tsunami sources employed for the development of the Arena Cove forecast model. Those highlighted in red are more extensively investigated using the reference model.
Figure 5. A sample interval from the Arena Cove tsunami-capable tide gage.
Figure 6. The setting of the Arena Cove model.
Figure 7. Nested grid representation for the Reference Model (RM). Rectangles are drawn, when appropriate, to indicate the placement of the next nesting level.
Figure 8. Nested grid representation for the Forecast Model (FM). Rectangles are drawn, when appropriate, to indicate the placement of the next nesting level.
Figure 9. Illustration of the appearance of model instability (upper panel.) The RM C-grid bathymetry in this case required minor modifications, following which the "null" test gave satisfactory results.
Figure 10. Locations of synthetic tsunami scenarios employed in model development.
Figure 11. Comparison of Reference (RM) and Forecast (FM) model results for the ACSZ 56-65 synthetic mega-event, representing the Cascadia Subduction Zone. Time series at the tide gage location in Arena Cove are shown in the upper panel. The lower panels contrast the RM and FM amplitude and velocity fields at the time indicated. Insets are enlargements of Arena Cove.
Figure 12. As in Figure 11, but for the KISZ 01-10 scenario representing Kamchatka.
Figure 13. As in Figure 11, but for the NTSZ 30-30 scenario representing Samoa.
Figure 14. Comparison of the Reference and Forecast Model response to a synthetic moderate event at NTSZ B36 near Samoa.
Figure 15. Comparison of the RM and FM response for the historical Unimak-1946 tsunami (prior to Arena Cove tide gage.).
Figure 16. Comparison of the RM and FM response for the historical Alaska-1964 tsunamis (prior to Arena Cove tide gage.)
Figure 17. Comparison of RM and FM hind casts of the Kuril 2006 event to sea level fluctuations in Arena Cove, observed by the tsunami-capable tide gage.
Figure 18. Comparison of RM and FM hind casts of the Samoa 2009 event to sea level fluctuations in Arena Cove.
Figure 19. Comparison of RM and FM hind casts of the Chile 2010 event to sea level fluctuations in Arena Cove.
Figure 20. Simulated model response (FM) to the historical Sanriku 1896, Kamchatka 1952, Andreanof 1957 and Chile 1960 events. Proxy observations (in red) are provided where available from other California locations. The Sanriku 1896 result is not expected to match the observed run-up at nearby Mendocino. The state of the tide is shown and times are given as UTC.
Figure 21. Model response (FM) to the East Kuril 1994, Chile 1995, Kuril 1995 and Irian Jaya 1996 events. Tide gage data (in red) where available is from Arena Cove.

DRAFT

Figure 22. Model response (FM) to the Andreanof 1996, Peru 2001, Hokkaido 2003, and Rat Island 2003 events. Tide gage data (in red) are from Arena Cove.
Figure 23. Model response (FM) to the Tonga 2006, Kuril 2007, Solomons 2007, and Peru 2007 events. Tide gage data (in red) are from Arena Cove.
Figure 24. Model response (FM) to the Chile 2007, Papua-New Guinea 2009, Solomons 2009, and Vanuatu 2009 events. Tide gage data (in red) are from Arena Cove.
Figure 25. Model response (FM) to the Samoa 2009 and Chile 2010 events. Tide gage data (in red) are from Arena Cove.
Figure 26. Seismicity in the vicinity of Cape Mendocino and the source mechanisms of notable recent earthquakes, adapted from USGC/NEIC products. The lower panel shows the poor agreement between the model and Arena Cove tide gage observations that is likely due to inadequate source representation in the model.
Figure 27. Comparison of FM real-time forecast and RM hindcast of the Honshu 2011 event with sea level observations in Arena Cove.
Figure 28. Predicted maximum sea level (from the FM) at the Arena Cove tide gage for the "mega-event" scenarios described in Table 6. Great circle routes are shown in red (with distances in km), and black arrows indicate the normal to the strike direction.
Figure 29. Comparison of RM and FM predictions for inundation of the Arena Cove / Manchester Beach region for selected mega-tsunami scenarios, and (lower right) for the ensemble employed in the CalEMA study.

DRAFT

List of Tables

Table 1a. Source characterization for historical tsunami events employed in Arena Cove model testing. Those in bold text were used in RM/FM inter-comparison. Sources identified as "ad hoc" may not be identically defined in other Forecast Model reports.

Table 1b. Supplementary historical tsunami events employed for Arena Cove forecast model testing. Those identified as "ad hoc" and may not be identically implemented in other Forecast Model reports.

Table 2. The main features of the Arena Cove Digital Elevation Model.

Table 3. Tidal characteristics of the Arena Cove, CA Tide Gage (9416841).

Table 4. Specifics of the grids and model parameters employed to model Arena Cove, CA. "EWxNS" denotes the number of grid values in the zonal (East to West) and meridional (North to South) directions respectively.

Table 5. Grid file names and grid-related parameters. The time steps for the A and B-grids must be integer multiples of the basic time step chosen for the C-grid.

Table 6. Description of the synthetic tsunami scenarios. Details of the source zones and specifics of the individual unit sources are provided in Appendix B.

DRAFT

This page in intentionally blank.

DRAFT

PMEL Tsunami Forecast Series: Vol. NNNN
Development of a Tsunami Forecast Model for Arena Cove, California

Michael C. Spillane [1,2]

Foreword

Tsunamis have been recognized as a potential hazard to United States coastal communities since the mid-twentieth century, when multiple destructive tsunamis caused damage to the states of Hawaii, Alaska, California, Oregon, and Washington. In response to these events, the United States, under the auspices of the National Oceanic and Atmospheric Administration (NOAA), established the Pacific and Alaska Tsunami Warning Centers, dedicated to protecting United States interests from the threat posed by tsunamis. NOAA also created a tsunami research program at the Pacific Marine Environmental Laboratory (PMEL) to develop improved warning products.

The scale of destruction and unprecedented loss of life following the December 2004 Sumatra tsunami served as the catalyst to refocus efforts in the United States on reducing tsunami vulnerability of coastal communities, and on 20 December 2006, the United States Congress passed the "Tsunami Warning and Education Act" under which education and warning activities were thereafter specified and mandated. A "tsunami forecasting capability based on models and measurements, including tsunami inundation models and maps." is a central component for the protection of United States coastlines from the threat posed by tsunamis. The forecasting capability for each community described in the PMEL Tsunami Forecast Series is the result of collaboration between the National Oceanic and Atmospheric Administration office of Oceanic and Atmospheric Research, National Weather Service, National Ocean Service, National Environmental Satellite Data and Information Service, the University of Washington's Joint Institute for the Study of the Atmosphere and Ocean, National Science Foundation, and United States Geological Survey.

Abstract. Operational tsunami forecasting by NOAA's Tsunami Warning Centers relies on the detection of tsunami wave trains in the open ocean, the inversion of these data (telemetered via satellite) to quantify their source characteristics, and real-time modeling of the impact on threatened coastal communities. The latter phase of the process involves, for each such community, a pre-tested Forecast Model capable of predicting the impact, in terms of inundation and dangerous inshore currents, with sufficient resolution and within the time constraints appropriate to an emergency response.

In order to achieve this goal, considerable advance effort is required to tune each forecast model to the specific bathymetry and topography, both natural and manmade, of the impact area, and to validate its performance with a broad set of tsunami sources. Where possible the validation runs should replicate observed responses to historical events, but the sparse instrumental record of these rare but occasionally devastating occurrences

DRAFT

dictates that comprehensive testing should include a suite of scenarios that represent potential future events.

During the forecast model design phase, and in research mode outside the pressures of an emergency situation, more detailed and slower-running models can be investigated. Such a model, referred to as a Reference Model, represents the most credible numerical representation of tsunami response for the study region, using the most detailed bathymetry available and without the run-time constraint of operational use. Once a reference model has been developed, the process of forecast model design is to determine where efficiencies can be gained, through reducing the grid resolution and increasing the model time step, while still adequately representing the salient features of the full solution.

This report documents the reference and forecast model development for Arena Cove, a small inlet south of the rocky Arena Point headland in southern Mendocino County, CA. Both the cove and the headland serve as reference points in coastal reports and are tourist venues but, while several tsunami have been detected by the tide gage there, no injury or infrastructure damage have been reported to date. The Manchester Beach area, north of Point Arena, is low-lying and subject to inundation and has been included in the model domain.

[1] Joint Institute for the Study of the Atmosphere and Ocean (JISAO), University of Washington, Seattle, WA
[2]NOAA/Pacific Marine Environmental Laboratory (PMEL), Seattle, WA

DRAFT

1.0 Background and Objectives

1.1. The Setting

Arena Cove is a semi-circular indentation, some 450 meters in diameter flanked by cliffs, lying south of the rocky headland whose northernmost point is the site of the Point Arena lighthouse. The cove appears about one-third of the way above the lower edge of Figure 1 (based on the 2005 NAIP Imagery for USGS 7.5min quadrangle: 38123h6, available online at atlas.ca.gov/quads). Apart from a pier (better seen in Figure 2), raised high above water level on pilings and the focus of local commercial fishing and tourist activity, the waterfront area of Arena Cove is almost devoid of infrastructure though it lies within the city limits of Point Arena. This small city has a population of about 500, who mainly reside at elevations that place them above the level likely to be impacted by even the most severe tsunamis. Population is sparse both to the south and north of Point Arena but inundation of Manchester Beach State Park, north of the lighthouse, and the low-lying area near the mouth of the Garcia River (crossed by State Highway 1), needs consideration. A comprehensive study of potential tsunami inundation, for the entire California coastline, was conducted by the University of Southern California Tsunami Research Center. Funded through the California Emergency Management Agency (CalEMA), by the National Tsunami Hazard Program, the study (Barberopoulou et al, 2011) has produced a set of inundation maps for emergency planning purposes accessible online in various forms, including a tool MyHazard (myhazards.calema.ca.gov) enabling users to acquire information specific to their site of interest. The CalEMA inundation results are available in GIS form and those specific to the Arena Cove area are used throughout this report. In addition to underpinning the modeling effort, the digital elevation model (DEM) for the region, provided by the National Geophysical Data Center (NGDC), includes a 3-D oblique view that assists greatly in visualizing the study area. In Figure 3, the CalEMA inundation information is overlaid, together with descriptive labels on an extract from the NGDC image, available in full in the DEM Report (Friday et al., 2009).

Arena Cove, both in appearance (Figure 2) and population, has not changed substantially since the nineteenth and early twentieth centuries, when it was one of the "Dog Hole" ports of the Mendocino Coast (Haugan, 2005). So named for their small size, these ports nonetheless served an important role in the provision of lumber in the building of the cities of California, and in the rebuilding of San Francisco in the wake of the 1906 earthquake and fire (see the inset to Figure 2, reproduced by permission of the Mendocino County Historical Society.) The Point Arena lighthouse, and its namesake city, were seriously damaged by the earthquake and the San Andreas Fault (SAF) dominates the local topography. The SAF intersects the coast just north of Point Arena en route to the triple junction near Cape Mendocino, the southern limit of the Cascadia Subduction Zone, which constitutes a major earthquake and tsunami hazard to the U.S. west coast.

Unlike the other ports of the Mendocino Coast, whose mouths have sand bars, the channeling northward of the Garcia River by the SAF, leaves a limited watershed to

DRAFT

supply sediment to Arena Cove via Point Arena Creek entering the cove through a small, steep-sided valley. The current pier, rebuilt in 1986 following the damage to its predecessor by a series of storms in 1983, stands on pilings high above water level. It houses a crane to lower boats to the water and the instrumentation for the tide gage whose sensor is adjacent to the pier. In earlier days piers, and wire chutes atop the flanking cliffs, delivered lumber products to coastal schooners. Today's pier supports local commercial fishing and sightseeing, surfing and pier fishing are popular tourist activities.

Apart from the pier, and some riprap, the cove remains in its natural state. A congressional study (U.S. Secretary of War, 1914) considered the possibility of engineering works to make Arena Cove a "harbor of refuge" between San Francisco and Humboldt Bay but concluded that this was neither feasible nor a serious need. Consequently sea level data from the tide gage represents coastal conditions, unaffected by infrastructure. Port Road links the pier, the parking area, and some buildings housing fishing and tourist amenities, to the city proper. Accommodations, in the immediate pier area, are confined to an inn that is well elevated from the waves associated with winter storms and, as this report will document, even the most severe tsunami.

South of Arena Cove, as illustrated in a striking series of aerial photographs (www.californiacoastline.org the source of the main frame of Figure 2), high cliffs limit potential impact by tsunamis. To the north of the lighthouse however, and stretching as far as the Irish Beach community, lies Manchester Beach State Park. Inland from the point of entry to the ocean of the Garcia River, is the Manchester-Point Arena Rancheria of the federally recognized Band of Pomo Indians. While the historical record of tsunamis does not include mention of this area, its risk for inundation is evident in the CalEMA chart and the results of this study indicate that it may be prone to inundation in severe tsunami events. Thus, while the study focuses on Arena Cove, and the validation of the forecast model is provided by the tide gage there, the analysis of the most severe scenarios will consider potential impacts to the Manchester area. The community of Manchester itself appears to be immune to direct impact, though the State Highway 1 (also called the Shoreline Highway) may be inundated where it crosses the Garcia River. Queries to the CalEMA "MyHazards" site for Point Arena and Manchester show flooding and earthquake as other hazards to which they are prone, in addition to tsunami.

1.2. Natural Hazards

Several instances of mild tsunami signals are evident in the tide gage records for Arena Cove, whose name appears several times in the records compiled by Lander and Lockridge (1989) and the NGDC Tsunami Hazard Database (Dunbar, 2007; see www.ngdc.noaa.gov/hazard/). The historical record first mentions Mendocino County with a 1-meter wave height associated with the Sanriku event of 1896. O'Brien (1946) described a 2.4 meter wave (4.3m above MLLW) at Arena Cove during the 1946 Unimak tsunami. At Noyo Harbor (adjacent to Fort Bragg, the largest coastal community in the county; 2010 population 7,273) "100 fishing boats thrown 1.8m up beach and some damage to pier." While Arena Cove was not explicitly mentioned in connection with the 1957 Andreanof event there was a report from Noyo Harbor. Similarly during the 1960

DRAFT

Chile event, "6 boats broke mooring … pier damaged" at Noyo Harbor and a height of 0.61m was observed at Gualala River near the southern boundary of Mendocino County. During the 1964 Alaska tsunami a run-up height of 1.83 meters occurred at Arena Cove and several instances of mild response to tele-tsunamis are available, following the installation of a tide gage in 1978, with which to validate model predictions.

The M_w 7.2 earthquake north of Cape Mendocino on April 25, 1992 was a very mild foretaste of a Cascadia Subduction Zone (CSZ) event. It produced wave heights of 0.14m at Arena Cove and 0.50m at Crescent City. Large-scale events on the CSZ are simulated later in the report but the weak 1992 event will be examined to see whether the presence of the Point Arena headland provides protection to Arena Cove, which lies in its lee for waves propagating along the coast from the north.

Combining events impacting northern California with those that have occurred since the Arena Cove tide gage was upgraded to 1-minute sampling, a total of 27 historical events are available for study. Nineteen of these, listed in Table 1a, are the standards for forecast model testing in the Pacific because their sea floor deformation is reasonably well known, either from the literature or, more recently, derived from direct observation of the wave trains they generated. The remaining eight, listed in Table 1b, have source characteristics that are less well known; they are included to expand the geographical coverage or because of their special relevance to Arena Cove. The Mendocino-1992 event for example was the most recent subduction-type event in Cascadia. Others, due to significant noise in the tide gage, do not produce a clear signal but shed light on Arena Cove as a reference point for coastal impacts. Figure 4 illustrates the distribution of the 27 historical sources. Those highlighted in red were employed for intercomparison of the reference and forecast versions of the model.

Direct seismic impact is another natural hazard to which Point Arena area is exposed. Its proximity to the rupture zone of the SAF in the San Francisco earthquake of 1906 resulted in significant damage to the town and the destruction of the lighthouse. While the SAF enters the ocean at Manchester Beach, its strike-slip nature reduces the likelihood of severe tsunami wave generation should ruptures occur in the immediate vicinity. Submarine landslides or collapse of sections of sea cliff are a potential local source for tsunami damage. Landslides triggered by seismic events caused significant loss of life during the 1929 Newfoundland event and accentuated the 1996 New Guinea tsunami. Landslide-generated tsunami waves are not currently included in the SIFT forecast methodology, nor are those generated meteorologically. However, to the extent that the waves they produce are detected by the DART® array, some warning of their presence may be available.

DRAFT

Table 1a. Source characterization for historical tsunami events employed in Arena Cove model testing. Those in bold text were used in RM/FM inter-comparison. Sources identified as "ad hoc" may not be identically defined in other Forecast Model reports.

Earthquake / Seismic				Model		
Event	**USGS Date Time (UTC) Epicenter**	**CMT Date Time (UTC) Centroid**	**Magnitude M_w**	**Tsunami Magnitude**	**Subduction Zone**	**Tsunami Source (Reference/Derivation)**
1946 Unimak	01 Apr 12:28:56 52.75ºN 163.50ºW	Not Available	8.5	8.5	ACSZ	7.5×B23 + 19.7×B24 + 3.7×B25 (López & Okal, 2006)
1952 Kamchatka	04 Nov 16:58:26.0 52.76ºN 160.06ºE	Not Available	9.0	9.0	KISZ	19.71 × (A4 + Y4 + Z4 + A5 + Y5 + Z5 + A6 + Y6 + Z6) (ad hoc)
1957 Andreanof	09 Mar 14:22:31 51.56ºN 175.39ºW	Not Available	8.6	8.7	ACSZ	31.4×A15 + 10.6×A16 + 12.2×A17 (Preliminary)
1960 Chile	22 May 19:11:14 38.29ºS 73.05ºW	Not Available	9.5	9.5	CSSZ	125×(A93 + B93 + Z93 + A94 + B94 + Z94 + A95 + B95) Kanamori & Cipar (1974)
1964 Alaska	28 Mar 03:36:00 61.02ºN 147.65ºW	Not Available	9.2	8.9	ACSZ	15.4×A34 + 18.3×B34 + 48.3×Z34 +19.4×A35 +15.1×B35 (Tang et al., 2006, 2009)
1994 East Kuril	04 Oct 13:22:58 43.73ºN 147.321ºE	04 Oct 13:23:28.5 43.60ºN 147.63ºE	8.3	8.1	KISZ	9.0×A20 (ad hoc)
1996 Andreanof	10 Jun 04:03:35 51.56ºN 175.39ºW	10 Jun 04:04:03.4 51.10ºN 177.410ºW	7.9	7.8	ACSZ	2.40×A15 + 0.80×B16 (Preliminary)
2001 Peru	23 Jun 20:33:14 16.265ºS 73.641ºW	23 Jun 20:34:23.3 17.28ºS 72.71ºW	8.4	8.2	CSSZ	5.7×A15 + 2.9×B16 + 1.98×A16 (Preliminary)
2003 Hokkaido	25 Sep 19:50:06 41.775ºN 143.904ºE	25 Sep 19:50:38.2 42.21ºN 143.84ºE	8.3	8.3	KISZ	3.95 × (A22 + B22 + A23 + B23) (ad hoc)
2003 Rat Island	17 Nov 06:43:07 51.13ºN 178.74ºE	17 Nov 06:43:31.0 51.14ºN 177.86ºE	7.7	7.8	ACSZ	2.81×B11 (Real-time)
2006 Tonga	03 May 15:26:39 20.13ºS 174.161ºW	03 May 15:27:03.7 20.39ºS 173.47ºW	8.0	8.0	NTSZ	6.6×B29 (ad hoc)
2006 Kuril	15 Nov 11:14:16 46.607ºN 153.230ºE	15 Nov 11:15:08 46.71ºN 154.33ºE	8.3	8.1	KISZ	4.0×A12 + 0.5×B12 + 2.0×A13 + 1.5×B13 (Real-time)
2007 Kuril	13 Jan 04:23:20 46.272ºN 154.455ºE	13 Jan 04:23:48.1 46.17ºN 154.80ºE	8.1	7.9	KISZ	-3.64 × B13 (Real-time)
2007 Solomon	01 Apr 20:39:56 8.481ºS 156.978ºE	01 Apr 20:40:38.9 7.76ºS 156.34ºE	8.1	8.2	NVSZ	12.0×B10 (Preliminary)
2007 Peru	15 Aug 23:40:57 13.354ºS 76.509ºW	15 Aug 23:41:57.9 13.73ºS 77.04ºW	8.0	8.1	CSSZ	0.9×A61 + 1.25× B61 + 5.6×A62 + 6.97×B62 + 3.5×Z62 (Preliminary)
2007 Chile	14 Nov 15:40:50 22.204ºS 69.869ºW	14 Nov 15:41:11.2 22.64ºS 70.62ºW	7.7	7.6	CSSZ	1.65×Z73 (Real-time)
2009 Samoa	29 Sep 17:48:10 15.509ºS 172.034ºW	29 Sep 17:48:26.8 15.13ºS 171.97ºW	8.1	8.1	NTSZ	3.96×A34 + 3.96×B34 (Real-time)
2010 Chile	27 Feb 06:34:14 35.909ºS 72.733ºW	27 Feb 06:35:15.4 35.95ºS 73.15ºW	8.8	8.8	CSSZ	17.24×A88 + 8.82×A90 + 11.84×B88 + 18.39×B89 + 16.75×B90 + 20.78×Z88 + 7.06×Z90 (Real-time)
2011 Honshu	11 Mar 05:46:24 38.297^{0}N 142.372^{0}E	11 Mar 05:47:47.2 38.486^{0}N 142.597^{0}E	9.0	9.0	KISZ	4.66 × B24 + 12.23×B25 + 26.31×A26 + 21.27×B26 + 22.75×A27 + 4.98×B27 (Real-time; Tang et al., 2012)

DRAFT

Table 1b. Supplementary historical tsunami events employed for Arena Cove forecast model testing. Those identified as "ad hoc" and may not be identically implemented in other Forecast Model reports.

Earthquake / Seismic				Tsunami Source (Reference/Derivation)		
Event	**USGS Date Time (UTC) Epicenter**	**CMT Date Time (UTC) Centroid**	**Magnitude M_w**	**Tsunami Magnitude**	**Subduction Zone**	**Tsunami Source**
1896 Sanriku	15 Jun 10:33:00 39.5ºN 144.0ºE		7.6	7.6	KISZ	b25 x 1.413 (ad hoc)
1992 Mendocino	25 Apr 18:06:04 40.368ºN 124.316ºW	25 Apr 18:06:11.8 38.56ºN 123.31ºW	7.2	7.2	ACSZ	a65 x 0.355 **or** b65 x 0.355 (ad hoc)
1995 Chile	30 Jul 05:11:24 23.340ºS 70.294ºW	30 Jul 05:11:56.9 24.17ºS 70.74ºW	8.0	8.0	CSSZ	2.812 x (a75 + b75) (ad hoc)
1995 Kuril	03 Dec 18:01:09 44.663ºN 149.300ºE	03 Dec 18:01:36.1 44.82ºN 150.17ºE	7.9	7.9	KISZ	1.991 x (a17 + z17) (ad hoc)
1996 Irian Jaya	17 Feb 05:59:31 0.891ºS 136.952ºE	17 Feb 06:00:02.8 0.67ºS 136.62ºE	8.2	8.2	NGSZ	2.7984 x (a9 + b9 + a10 + b10) (ad hoc)
2009 PapuaNG	03 Jan 19:43:51 0.414ºS 132.885ºE	03 Jan 19:44:09.0 0.38ºS 132.83ºE	7.6	7.6	NGSZ	0.7046 x (b13 + b14) (ad hoc)
2009 Kuril	15 Jan 17:49:39 46.857ºN 155.154ºE	15 Jan 17:49:48.3 46.97ºN 155.39ºE	7.4	7.4	KISZ	b12 x 0.7063 (ad hoc)
2009 Vanuatu / Santa Cruz	07 Oct 22:03:15 13.052ºS 166.187ºE	07 Oct 22:03:28.9 12.59ºS 166.27ºE	7.6	7.6	NVSZ	1.2×B24 + 0.26×A23 *followed after 15minutes by*
	07 Oct 22:18:26 12.554ºS 166.320ºE	07 Oct 22:19:15.3 11.86ºS 166.01ºE	7.8	7.9	NVSZ	2.6×B23 + 0.9×A23 (Preliminary Wei 2009, Personal Communication)

DRAFT

Another local hazard that has been a frequent cause of damage to Arena Cove has been ocean wave action. Originating locally, or as swell from distant storms, such waves caused severe damage to the pier in 1983 that necessitated its replacement. Another impact of ocean waves, of relevance to tsunami detection and modeling, is in the noise they produce in the tide gage record that can mask weaker tsunami signals, Harbor resonance in the case of Crescent City can amplify the tsunami and may be a factor too in the Arena Cove response.

1.3. Tsunami Warning and Risk Assessment

The forecast model development, described here, will permit Arena Cove, CA, to be incorporated into the tsunami forecasting system SIFT, developed at NCTR (NOAA Center for Tsunami Research) and now in operational use at the U.S. Tsunami Warning Centers (TWC's). The system has had considerable success is accurately forecasting the impact of both moderate and severe tsunami events in recent years and in the following section the methodology that permits such forecasts is discussed as prelude to a description of development of the forecast model for Arena Cove. With the model in hand, validated with historical events and with its stability verified by extensive testing against extreme scenarios, real-time forecasts will be available to inform local emergency response. Additionally, the synthetic scenarios investigated during model development, and reported here, provide an initial tsunami risk assessment as described in the Results and Discussion section.

DRAFT

2.0 Forecast Methodology

2.1 The Tsunami Model

In operational use, a tsunami forecast model is used to extend a pre-computed deep-water solution into the shallows, and onshore as inundation if appropriate. The model consists of a set of three nested grids, of increasingly fine resolution that, in a real-time application of the MOST model (Method of Splitting Tsunami: Titov and Synolakis, 1998; Titov and González, 1997), permits forecasts at spatial scales (as little a few tens of meters) relevant to local emergency management. The validity of the MOST model applied in this manner, and the operational effectiveness of the forecast system built around it, has been demonstrated during unplanned tests triggered by several mild to moderate tsunami events in the years since the 2004 Indian Ocean disaster (Wei et al., 2008). Successful hindcasting of observed historic events, even mild ones, during forecast model development lends credence to the ability to accurately forecasting the impact of future events. Such validation of tsunami modeling procedures is documented in other volumes of the series of which this report is but one. Before proceeding to a description of the forecast model development for Arena Cove, it is useful to describe the steps in the overall forecast process.

2.2 The SIFT Forecast System

Operational tsunami forecasts are generated at Tsunami Warning Centers, staffed 24/7 in Alaska and Hawaii, using the SIFT (Short-term Inundation Forecasting for Tsunamis) tool, developed at NCTR. The semi-automated process facilitates the steps by which TWC operators assimilate data from an appropriate subset of the DART® tsunami sensors, "invert" the data to determine the linear combination of pre-computed propagation solutions that best match the observations, then initiate a set of forecast model runs if coastal communities are threatened or, if warranted, cancel the warning.

Steps in the process are as follows:

- When a submarine earthquake occurs the global network of seismometers registers it. Based on the epicenter, the unit sources in the Propagation Database (Gica et al., 2008) that are most likely to be involved in the event, and the DART® array elements (Spillane et al., 2008) best placed to detect the waves passage are identified. TWC watch-standers can trigger DART®s into rapid sampling mode in the event that this did not occur automatically in response to the seismic signal.
- There is now an unavoidable delay while the tsunami waves are in transit to the DART®s; at least a quarter of a cycle of the first wave in the train must be sampled before moving to the "inversion" step.
- When sufficient data have accumulated, at one or more DART®s, the observed time series are compared with the model series from the candidate unit sources. Since the latter are pre-computed (using the MOST code), and the dynamics of tsunami waves in deep water is linear, a least squares approach taking very little time can identify the unit sources, (and the appropriate scale factors for each,) that

DRAFT

best fit the observations. The "inversion" methodology is described by Percival et. al., (2009).

- Drawing again on the Propagation Database, the scale factors are applied to produce a composite basin-wide solution with which to identify the coastal regions most threatened by the radiating waves.
- It is at this point that one or more forecast models are run. The composite propagation solution is employed as the boundary condition to the outermost (A-grid) domain of a nested set of three real-time MOST models that telescope with increasingly fine scale to the community of concern. A-grid results provide boundary conditions to the B-grid, which in turn forces the innermost C-grid. Non-linear processes including inundation are modeled so that, relying on the validation procedures during model development, credible forecasts of the current event are available.
- Each forecast model provides quantitative and graphic forecast products with which to inform the emergency response, or to serve as the basis for canceling or reducing the warnings. Unless the tsunami source is local, the forecast is generally available before the waves arrive but, even when lead-time cannot be provided, the several hour duration of a significant event (in which the first wave may not be the most damaging) give added value to the multi-hour forecasts provided.

Because multiple communities may be potentially at risk, it may be necessary to run simultaneously, or in a prioritized manner, multiple forecast models. Each must be optimized to run efficiently in as little time as possible; the current standard is that an operational forecast model should be capable of simulating 4 hours of real time within about 10 minutes of CPU time on a fast workstation computer.

DRAFT

3.0 Model Development

3.1 Digital Elevation Models

Water depth determines local tsunami wave speed and sub-aerial topography determines the extent to which tsunami waves inundate the land. Thus a prerequisite for credible tsunami modeling is the availability of accurate gridded bathymetric and topographic datasets, termed DEM's (Digital Elevation Models.) Given their expertise in this area, and the number of coastal communities needing tsunami forecast capability, NCTR relies heavily on the National Geophysical Data Center (NGDC) to provide the DEM's needed. In the case of Arena Cove, the DEM, a composite of multiple data sources merged and converted to a common datum of Mean High Water (MHW), was produced and documented by Friday et al. (2009). The use of MHW as the "zero level" for forecast results is standard. The MOST model does not include tidal fluctuations and, since a tsunami may arrive at any stage of the tide, it is best to employ a "worst-case" approach by assuming high tide when forecasting inundation. For some Forecast Models grounding of vessels and the strong and the rapidly varying currents often associated with even mild tsunamis are of concern. For Arena Cove, lacking a marina and shoreline infrastructure, low water impacts are less important.

Table 2. The main features of the Arena Cove Digital Elevation Model (DEM).

Grid Area	**Arena Cove, California**
Coverage Area	123.43º to 124.43º W; 38.40º to 39.40º N
Coordinate System	Geographic decimal degrees
Horizontal Datum	World Geodetic System 1984 (WGS84)
Vertical Datum	**Mean High Water (MHW)**
Vertical Units	Meters
Cell Size	**1/3 arc-second**
Grid Format	ESRI Arc ASCII grid

The DEM provided by NGDC for the Arena Cove area was illustrated in Figure 3; its salient features listed in Table 2 reproduced from DEM documentation (Friday et al., 2009). The NGDC report thoroughly describes the data sources and methods employed in constructing the DEM. With one-third arc second (~10m) resolution, the DEM provides the basis for the B and C-grids for both reference and forecast model usage. NCTR maintains an atlas of lower resolution gridded bathymetries, which can be used for the A-grids, as described later. All of the DEMs employed were verified for consistency with charts, satellite imagery, and other datasets during the course of MOST grid development.

DRAFT

3.2 Tides and Sea Level Variation

Arena Cove's history of tidal observations dates back only to 1978. The tide station (9416841, $38^0$54.8'N, $123^0$42.4'W) is located near the end of the pier whose concrete pilings raise the deck about 25 feet above sea level and do not impede water movement within the cove. The instrumentation was upgraded in 2006 to include a tsunami-capable gage sampling at 1-minute intervals; some earlier data was sampled at 6-minute intervals and several historical events are only available as marigrams on microfiche. An ongoing project at NGDC will digitize the more critical images in this archive.

Station characteristics for 9416841 are provided in Table 3, based on the wealth of online tidal information available at NOAA's CO-OPS (Center for Operational Oceanographic Products and Services) website (tidesandcurrents.noaa.gov). Note the sizeable diurnal range of over three meters and that, while the long-term rate of change in sea level is low (compared to more seismically active areas), there is substantial seasonal, interannual and short-term variability. Owing to the relative short history of the Arena Cove gage, trends and cycles are reported for Crescent City to the north and Point Reyes to the south.

Table 3. Tidal characteristics of the Arena Cove, CA Tide Gage (9416841).

Arena Cove, CA	**Station#9416841**		**$38^0$54.8'N, $123^0$42.4'W**
Tidal Datum and Range Values (Epoch 1983-2001)			
MHHW (Mean Higher High)	10.618m	Great Diurnal Range 1.792m	
MHW (Mean High Water)	10.413m		Mean Range 1.233m
MSL (Mean Sea Level)	9.786m		
MLW (Mean Low Water)	9.180m		
MLLW (Mean Lower Low)	8.826m		
Sea Level Trends and Cycles (from Point Reyes, CA #9415020)			
Long Term SL Trend	Increasing 2.10±1.52mm/year		
Seasonal Cycle Range	Minimum -89mm(April); Maximum 59mm(September)		
Interannual Variation (from1980)	Minimum -20mm(1988); Maximum +21mm(1997)		
Sea Level Trends and Cycles (from Crescent City, CA #9419750)			
Long Term SL Trend	Decreasing 0.65±0.36mm/year		
Seasonal Cycle Range	Minimum -87mm(May); Maximum 85mm(January)		
Interannual Variation (from1980)	Minimum -20mm(1989); Maximum +28mm(1998)		

A sample section of the tide gage record, again extracted from the CO-OPS website is reproduced in Figure 5. Deviations (or residuals) from the astronomically predicted tide can be several centimeters and the variability strong. In particular the highest water level reported for the Arena Cove gage is 1.048m above MHW (Feb 6, 1998) so the use of MHW as the zero level of modeled sea level may underestimate the truly worse case.

DRAFT

While the simultaneous arrival of the crest of a large tsunami at high tide during a storm surge has low probability, a feature of the simulated events reported below is that sustained oscillations at a resonant period may extend the duration of the threat. This effect is notorious at Crescent City, CA which is frequently the most heavily impacted U.S. west coast location for remote events.

3.3 The CFL Condition and other considerations for grid design

Water depth dependent wave speed, in conjunction with the spacing of the spatial grid representation, place an upper limit on the time step permissible for stable numerical solutions employing an explicit scheme. This is the CFL limit (Courant-Friedrichs-Levy), which requires careful consideration when the grids employed for a reference or forecast model are being designed. Finer-scale spatial grids, or greater water depths, require shorter time steps thereby increasing the amount of computation required to simulate a specific real time interval.

Another feature of the application of gridded numerical solutions to the tsunami wave problem is the shortening that the wave train encounters in moving from deep water onto the shelf. In deep water a grid spacing of 4 arc-seconds (of latitude and longitude, corresponding to ~7km) is normally used to represent propagating wave trains whose wavelength is typically of the order of a few hundred kilometers. The stored results of such propagation model runs are typically decimated by a factor of 4, resulting in a database of ~ 30km spacing (and 1 minute temporal sampling) with which to generate the boundary conditions for the outermost of the nested grids in a model solution. The extraction of the boundary conditions (of wave height and the two horizontal velocity components) is achieved by linear interpolation in space and time. To provide realistic interpolated values the stored fields for these variables must be smoothly varying, and have adequate sampling in space and time to resolve their structure. This necessitates the placement of the offshore boundary of the forecast model domain well offshore. The presence of the Mendocino Escarpment is another incentive to do so, in order that its role in topographic steering of trans-Pacific wave trains be adequately represented.

Figure 6 illustrates the placement of the model domain in its west coast setting. The outermost A-grid covers the entire region shown; embedded in it is the B-grid, which covers most of Mendocino County. The innermost C-grid, with the finest spatial resolution spans the region north and south of Point Arena. Marked in red are a number of nearby communities where run-ups are mentioned in the historical record. Indicated as black triangles are the tsunami-capable tide gages of the region, the closest of which are Point Reyes to the south and North Spit to the north. Almost directly offshore is DART® 46411. This would play a major role in the detection of regionally generated waves. Its offshore location cleanly registers moderate to large tele-tsunamis and could, potentially, refine a local forecast that was initially based on DART® array elements closer to the source. Red, green, and magenta lines indicate (using the color-convention employed in the online USGS/NEIC earthquake resources) the three types of fault that radiate from the triple junction off Cape Mendocino. To the south is the strike-slip San Andreas Fault, skirting the coastline north of San Francisco Bay before entering the ocean within the C-

DRAFT

grid domain. The Mendocino Escarpment is dramatic evidence of the ridge fault extending offshore but of most concern as a local source of tsunamis is the Cascadia Subduction Zone. The two southernmost pairs of the unit source set used to represent it fall within the A-grid domain. A "beachball," that visually represents the source mechanism, marks the location of the Mendocino-1992 event which was the last significant subduction event in Cascadia.

3.4 Specifics of the model grids

After several rounds of experimentation, the extents and resolutions of the nested grids were chosen, and are illustrated in Figures 7 and 8; details are provided in Tables 4 and 5. The Reference Model (RM) and Forecast Model (FM) grid pairs (at the A and B levels) have the same extent, differing only in resolution; the C-grid domain is however slightly larger for the RM than for the FM, the dimensions of the latter being reduced to achieve a shorter run-time appropriate to operational use. The corresponding panels in the figures employ the same depth contours and color palette, which consequently are only shown in the FM version (Figure 8). Rectangles drawn in red for the A and B grid panels, indicate the extent of the embedded grid; where appropriate the blue rectangles indicate the less extensive FM C-grid. Superimposed in the C-grid panels is the network of rivers, creeks and roads. The thick red line marks State Hwy 1, also called the Shoreline Highway.

Table 4. Specifics of the grids and model parameters employed to model Arena Cove, CA. "EWxNS" denotes the number of grid values in the zonal (East to West) and meridional (North to South) directions respectively.

Grid	**Zonal Extent (W)**		**Meridional Extent (N)**		**Resolution (")**		**Values EW x NS**	
					RM	**FM**	**RM**	**FM**
A	128.00^0	121.50^0	36.00^0	42.50^0	30	60	781x781	391x391
B	124.55^0	123.00^0	38.35^0	39.80^0	6	24	931x871	234x291
C	123.85^0	123.60^0	38.82^0	39.03^0	1	2	901x757	235x313
	123.78^0	123.65^0	38.89^0	39.02^0				

Table 5. Grid file names and grid-related parameters. The time steps for the A and B-grids must be integer multiples of the basic time step chosen for the C-grid.

Grid	Filename	Maximum Depth (m)	Minimum CFL (s)	Model Time Step (s)	Water Cells
A	ArenaCoveCA_RM_A	5002	3.350	3.0 (5x)	436966
	ArenaCoveCA_FM_A	5005	6.689	6.0 (4x)	109323
B	ArenaCoveCA_RM_B	3781	0.7559	0.6 (1x)	485760
	ArenaCoveCA_FM_B	3776	2.893	1.5 (1x)	40535
C	ArenaCoveCA_RM_C	143.6	0.6423	0.6	434701
	ArenaCoveCA_FM_C	94.4	1.526	1.5	37611

DRAFT

Both C-grids lie entirely within the NGDC-provided Arena Cove DEM; A and B-grids incorporate bathymetric and topographic from other DEM datasets available at NCTR. Some smoothing and editing were necessary to eliminate erroneous points or grid features that tend to cause model instability. For example, "point" islands where an isolated grid cell stands above water are eliminated, as are narrow channels or inlets one grid unit wide; these tend to resonate in the numerical solution. Large depth changes between adjacent grid cells can also cause numerical problems; customized tools (such as "bathcorr") are available to correct many of these grid defects.

Details of the model grids are provided in Tables 4 and 5. The latter lists the maximum depth, the CFL time step requirement that must not be exceeded, and the actual time steps chosen for the reference and forecast model runs. Since in the current version of MOST, employed by SIFT, the numerical solutions in the three grids proceed simultaneously, there is a requirement that the A and B-grid time steps be integer multiples of the (innermost) C-grid time step in addition to satisfying the appropriate CFL requirement. For both reference and forecast models the CFL requirement of the C-grid was the most stringent. The values chosen are shown in the final column of Tables 4 and 5 and are such that an integer multiple of each time step (16x for the forecast model; 64x for the reference) is identically 30 seconds, the chosen output time interval for both models. When run on an Intel® Xeon® E5670 2.93GHz processor, the forecast model can simulate four hours in 10.73 minutes, close to the desired value of 10-minutes for this metric.

3.5 Model Run Input and Output Files

In addition to providing the bathymetry file names and the appropriate time step and A, B grid multiples as provided in the tables above, the designer must provide a number of additional parameters in an input file. These include the Manning Friction Coefficient, a depth threshold to determine when a grid point becomes inundated, and the threshold amplitude at the A-grid boundary that will start the model. An upper limit is specified in order to terminate the run if the wave amplitude grows beyond reasonable expectation. Standard values are used: 0.0009 for the friction coefficient and 0.1m for the inundation threshold. The latter causes the inundation calculation to be avoided for insignificant water encroachments that are probably below the uncertainty in the topographic data. Inundation can, optionally, be ignored in the A and B-grids, as is the norm in the (non-nested) MOST model runs that generate the propagation database. When A and/or B-grid inundation is excluded, water depths less than a specified "minimum offshore depth" are treated as land; in effect a "wall" is placed at the corresponding isobath. When invoked, a value of 5m is applied as the threshold, though A and B inundation is normally permitted as a way to gain some knowledge of tsunami impact beyond the scope of the C-grid domain. Other parameter settings allow decimation of the output in space and/or time. As noted earlier, 30-second output has been the target and output at every spatial node is preferred. These choices avoid aliasing in the output fields that may be suggestive of instability (particularly in graphical output), when none in fact exists.

Finally the input files (supplied in Appendix A for both the reference and forecast versions of the model) provide options that control the output produced. Output of the

DRAFT

three variables: wave amplitude, and the zonal (positive to the east) and meridional (positive to the north) velocity components can be written (in netCDF format) for any combination of the A, B, and C-grids. These files can be very large! A separate file, referred to as a "SIFT" file, contains the time series of wave amplitude at each time step at discrete cells of a selected grid. Normally the time series at a "reference" or "warning point", typically the location of a tide gage is selected to permit validation in the case of future or historical events. Also output in the SIFT file is the distribution of the overall minimum and maximum wave amplitude and speed in each grid. By contrast with the complete space-time results of a run, the SIFT file (also netCDF) is very compact and, if more than a single grid point is specified, a broader view of the response is provided.

By default two additional output files are generated: a listing file, which summarizes run specifications, progress, and performance in terms of run time. Also included in this file is information to determine the reason, should a run not start or terminate early. Finally a "restart" file is produced so that a run can be resumed, beginning at the time it ended, either normally or by operator intervention.

The input files described above are specific to the model itself. For an actual run, the program must be pointed toward the files that contain the boundary conditions of wave amplitude (HA), and velocity components (UA, VA), to be imposed at the A-grid boundary. Time varying conditions are generally extracted as a subset of a basin-wide propagation solution (either a single unit source or several, individually scaled and linearly combined) that mimic a particular event. These boundary-forcing files typically consist of 24 hours of values (beginning at the time of the earthquake), sampled at 1-minute intervals and available on a 16 arc-minute grid. Occasionally, for more remote seismic sources (or when delayed arrival of secondary waves due to reflections are a concern, as has been seen at Hawaii,) the time span of the propagation run available for forcing is extended beyond one day.

DRAFT

4.0 Results and Discussion

Before proceeding to an extensive suite of model runs, that explore the threat to the Point Arena area from various source regions, the stability of the model is tested in both low and extreme amplitude situations. The former we refer to as "null source" testing: where the boundary forcing is at such a low level (but not precisely zero of course) that the response is expected to be negligible. These tests can be highly valuable in revealing localized instabilities that may result from undesirable features in the discretized bathymetric representation. Inlets or channels that are only one grid cell wide may "ring" or resonate in a non-physical way in the numerical solution. An instability may not grow large enough to cause the model to fail but, in a run with typical tsunami amplitudes, may be masked by actual wave variability.

Forcing by extreme events should also be tested. In addition to the need to test model stability under such circumstances, there is a parameter in the input file that truncates the run if a prescribed threshold is exceeded. For operational use, the threshold must be set high enough so that an extreme event run is not unnecessarily terminated. Both tests should be done for test sources whose waves enter the model domain from different directions since, although stable for one set of incoming waves, an instability may be encountered for another. The "null" and "extreme" testing of the forecast and reference models is reported in the following subsections. Further evidence of stability is provided by the extensive set of scenarios, aimed at exploring the dependence of impact to source location, described later in the report, and in independent testing by other members of the NCTR team before the model is released for operational use.

4.1 The "Null" Tests

Three null test cases (see Table 6) were run representing sources in the western Aleutians, the Philippines, and south of Japan. Based on sources from the propagation database (Gica et al., 2008), their amplitudes were scaled down by a factor of 10,000 so as to mimic an M_w=4.8333 / Slip 0.0001m source rather than the M_w=7.5 / Slip 1m standard. A number of grid cells in the B and C grids emerged as potential sources of instability. These were generally minor indentations of the coastline, barely resolved by the grids, or narrow channels. Also to be looked for in further testing is the area northwest of the Point Arena Light when the rugged seabed reveals several past water level stands. A limited number of grid cells in the outermost (A) grid required correction. Generally these were associated with non-physical features in the topographic database, such as where a track of ship-based soundings were improperly merged with other data sources. After an iterative process of grid correction and retesting using these "null" sources, both of the reference (RM) and forecast model (FM) grids were deemed satisfactory and the testing of realistic events can begin. Figure 9 illustrates a step in the process where a deficiency in the RM grid generated a mild instability (in the EPSZ B19 micro-tsunami scenario – see Table 6) causing the RM time series at the reference point, initially in close agreement with the FM, to develop unrealistic, high frequency oscillations. Though still generally tracking the FM result, and not growing without bound, the feature could behave erratically in simulating real events. Modification of the

DRAFT

Table 6. Synthetic tsunami events employed in Arena Cove, CA model testing. The RM and FM solutions of those shown in bold text were inter-compared extensively.

Scenario Name	Source Zone	Tsunami Source	α [m]
Mega-tsunami (M_w 9.3) Scenario			
KISZ 1-10	**Kamchatka-Yap-Mariana-Izu-**	**A1-A10, B1-B10**	**25**
KISZ 22-31	Kamchatka-Yap-Mariana-Izu-Bonin	A22-A31, B22-B31	25
KISZ 32-41	Kamchatka-Yap-Mariana-Izu-Bonin	A32-A41, B32-B41	25
KISZ 56-65	Kamchatka-Yap-Mariana-Izu-Bonin	A56-A65, B56-B65	25
ACSZ 6-15	Aleutian-Alaska-Cascadia	A6-A15, B6-B15	25
ACSZ 16-25	Aleutian-Alaska-Cascadia	A16-A25, B16-B25	25
ACSZ 22-31	Aleutian-Alaska-Cascadia	A22-A31, B22-B31	25
ACSZ 50-59	Aleutian-Alaska-Cascadia	A50-A59, B50-B59	25
ACSZ 56-65	**Aleutian-Alaska-Cascadia**	**A56-A65, B56-B65**	**25**
CSSZ 1-10	Central and South America	A1-A10, B1-B10	25
CSSZ 37-46	Central and South America	A37-A46, B37-B46	25
CSSZ 89-98	Central and South America	A89-B98, B89-B98	25
CSSZ 102-111	Central and South America	A102-A111, B102-	25
NTSZ 30-39	**New Zealand-Kermadec-Tonga**	**A30-A39, B30-B39**	**25**
NVSZ 28-37	New Britain-Solomons-Vanuatu	A28-A37, B28-B37	25
MOSZ 1-10	ManusOCB	A1-A10, B1-B10	25
NGSZ 3-12	North New Guinea	A3-A12, B3-B12	25
EPSZ 6-15	East Philippines	A6-A15, B6-B15	25
RNSZ 12-21	Ryukus-Kyushu-Nankai	A12-A21, B12-B21	25
M_w 7.5 Scenario			
NTSZ B36	New Zealand-Kermadec-Tonga	B36	1
Micro-tsunami Scenario			
EPSZ B19	East Philippines	B19	0.01
RNSZ B14	Ryukus-Kyushu-Nankai	B14	0.01
ACSZ B6	Aleutian-Alaska-Cascadia	B6	0.01

DRAFT

RM bathymetry eliminated the problem, as seen in the lower panel, and "null" tests involving other sources (RNSZ B14 and ACSZ B6) did not reveal other issues.

4.2 The Extreme Case Tests

The record of tsunami impact on the northern California coast discussed later reveals that sources around the entire periphery of the Pacific can be felt. Indeed the catastrophic Indian Ocean tsunami of 2004 was detectable at Arena Cove as it was throughout the global ocean. A broad suite of 19 extreme events (so-called mega-tsunamis) whose locations are standard for testing of Pacific basin forecast models, are described in Table 6. Their locations are shown in Figure 10. To simulate each mega-tsunami source, ten A-B pairs of unit sources are used, with an evenly distributed slip of 25m. As described by Gica et al. (2008), each unit source represents a 100x50km area of the fault surface with the long axis parallel to the plate boundary. The B-row is shallowest, sloping from a nominal depth of 5km (unless a depth estimate has been provided by the USGS based on the earthquake catalogs), row-A is deeper, followed by rows Z, Y, X, … where appropriate. Thus, the extreme case sources represent 1,000 km long ruptures with a width of 100km; the corresponding magnitude is M_w=9.3.

Discussion of the entire set in greater detail is provided later in the report, once the validity of the Forecast Model has been established. Here we focus on a subset of three, highlighted in Figure 10 and Table 6, to contrast the Forecast Model (FM) with the more highly resolved Reference Model (RM). The results are presented in Figures 11-13, with the time series at the reference point (the Arena Cove tide gage) shown in the upper panel and the amplitude and current pattern at a selected time shown below. The black curve and red curves represent the RM and FM respectively; the green line identifies the time at which the comparison in the lower panel was made. Inset in the lower panels are enlargements of the area around Arena Cove and are left pixilated to reflect the discrete grid resolution.

It is noticeable that, in all three of the cases shown, the RM tends to oscillate longer and have somewhat larger amplitude than does the FM though the two solutions are in close agreement for the first few tsunami waves. This is likely a physical reality: the more highly resolved bathymetry and coastline of the RM providing greater scope for non-linear features or reflected waves to develop. This observation suggests a caveat to operational use of the FM: while accurate portrayal of the early history of an event is to be expected, the duration of the event and the amplitude of later waves may be under-estimated. Tide gage data will be needed to verify this conjecture, which is pursued later in the report.

The snapshot comparisons in the lower panels of Figures 11-12 are quite reasonable, illustrating that the solutions match not just at the reference point. It is worth noting too that, although the ACSZ 56-65 mega-event represents a massive Cascadia tsunami, the scale of the impact to the Arena Cove area (~ 3m) is not substantially greater than from trans-Pacific locations (KISZ 01-10 off Kamchatka and NTSZ 30-39 near Samoa.) The Crescent City response to the same synthetic Cascadia mega-event exceeds 10m (Arcas

DRAFT

and Uslu, 2010). It would appear that the energy propagated along shore to the south, perhaps with some sheltering by Cape Mendocino, is reduced and that perhaps the greatest impact to Arena Cove may be associated with source regions elsewhere in the Pacific basin.

In Figure 13 the comparison time was intentionally chosen later in the event as a counterexample. While the reference point amplitudes and nearby fields the FM and RM may be in reasonable agreement, the broader wave patterns may have substantial phase differences. The comparisons in these lower panels is restricted to the portion of C-grid area common to both models, There is a suggestion that the near shore velocity fields at the north and south FM boundaries differ somewhat from the RM for which these are internal points.

Before proceeding to validate the model with historical events, one other synthetic event is usual in the testing protocol: a mild source of magnitude 7.5 at a remote location. A single unit source near Samoa (NTSZ-B36) is employed and its representation by the RM and FM are compared in Figure 14. Such an event results in a response of about 2cm in Arena Cove sea level and there is excellent agreement between both model representations in the earlier portion of the event.

Overall, the close agreement between the first wave arrival time and waveform, and overall range of variation of the two model representations in synthetic scenarios (even though the amplitude and phase is not always well-matched for later waves) suggests that the forecast model is performing well, and that we can, with confidence, proceed to model real events.

4.3 Model Validation with Historical Events

We now proceed to examine how well the RM and FM solutions compare with observation for several historical cases: those highlighted in Table 1 and Figure 6. Since the observations are limited to the tide gage records or run-up reports in Arena Cove the purpose of the lower panels is only to illustrate the agreement between the models.

The results, displayed and described below, represent the large Unimak-1946 and Alaska-1964 events, and three more recent ones: Kuril-2006 (which has been extensively studied), Samoa-2009, and Chile-2010. The latter three occurred subsequent to the installation of an improved tide gage at Arena Cove. In a later subsection, the Honshu tsunami of March 11, 2011 is discussed. It occurred while this report was undergoing internal review at NCTR but the FM was available for use in real-time circumstances. There is another difference between the earlier and more recent events. Source characterization for the former is based on the literature with the source mechanism estimated from the seismic record. The Kuril-2006 event was the first substantial event for which direct observation of the tsunami wave train was available from multiple deep-water DART® sites. As such its source characteristics, and those for Samoa-2009, Chile-2010, and Honshu-2011 are better suited to tsunami modeling and forecast; those based on seismic data only may suffer from the defect that earthquakes differ in their ability to

DRAFT

generate tsunami waves. An extreme case of this is the Sanriku-1896 event, which is modeled and discussed briefly later in this report. It was a so-called "tsunami-earthquake" (Dudley and Lee, 1998), causing devastating losses in Japan despite its modest magnitude and scant warning in the form of ground motion.

Even in the case of source characterizations based on DART® detection and inversion, it should be borne in mind that perfect agreement between the model wave and observation is unlikely. For one thing, the DART® sites used in the inversion process may be well described by a linear combination of unit source functions, but their placement may limit the ability to predict basin-wide energy propagation. Ideally one might hope to refine the model solution in light of DART® observations closer to the impact site. The deep-water waves in the far field (for example 46411 in the case of Arena Cove) may however fall below the DART® detection threshold. Neither are the tide-gage observations, available for comparison with model prediction, perfect. They may include noise, possible amplified by harbor resonances and wind wave activity.

The Unimak-1946 and Alaska-1964 events were widely felt along the U.S. west coast, though the greatest impact was to the Hawaiian Islands. Reported run-ups at Arena Cove were 2.40 and 1.83 meters respectively, comparable in the case of Alaska-1964 (but somewhat lower for Unimak-1946), to the modeled responses shown in Figures 15 and 16. The RM and FM solutions match well, both in the time series in the upper panel and the amplitude and velocity field at the selected comparison time.

For the more recent events, where time series at Arena Cove permit direct inter-comparison with the RM and FM predictions, the results are presented in Figures 17-19. For the Kuril-2006 event, the reported 61cm run-up at Arena Cove exceeds, by a factor of about 2, the amplitude of the tide gage oscillations. Particularly for the early waves the model gives a reasonable representation of both the amplitude and timing of the observations. The time axis is in model hours and the discrepancy in the first wave arrival time is about 5 minutes, just 1% of its transoceanic travel time.

For Samoa-2009 the reported run-up at Arena Cove is 44cm, which may correspond to later in the record when harbor resonances may have been excited. For the early waves, the amplitude of the observations is closer to 20cm and, though it does reasonably well in predicting the early timing and the sequence of waves, the model underestimates the amplitude by about a third. For the Chile-2010 event the amplitude of the observations is replicated more closely. Again though, the reported run-up of 35cm is substantially greater than the greatest positive excursion of the de-tided observations as displayed.

Considering the above results, the main discrepancy appears to be the mismatch between reported run-up and the processed sea level time series. Some possible explanations come to mind. Run-up is defined as maximum elevation above the predicted tide, which may not include seasonal or meteorologically driven departures, which, as illustrated in Figure 5, can be several centimeters. Another possibility is that the overall maximum of the tide gage record may be aliased by high-frequency variability, which was smoothed somewhat by a 3-point running average in the preparation of these graphics.

DRAFT

4.4 Further Historical Simulations

The above analysis has documented good agreement between the forecast model and the slower running reference version. This permits us to simulate the balance of the historical cases where impacts to Arena Cove and northern California have been reported, and the remaining mega-tsunami scenarios with the forecast model alone. These runs are intended to further validate the stability of the FM but also provide some information on the exposure of the region to tsunamis generated at various points on the periphery of the Pacific.

In Figures 20-24 the full set of observed records at Arena Cove (or in some cases proxy sites) are compared with FM prediction. Also provided, for each event, is the state of the tide at Arena Cove. While probably of little concern for weak events, this may be a factor in the impact of larger ones. Reported run-up is included in each case though, as noted earlier, this may be only loosely related to the plotted series. In each case, the FM series is shown in black; the observations are drawn in red. Although studies of the global ocean response to the Indian Ocean tsunami of December 2004 suggest a run-up of 19 cm in Arena Cove, the signal is largely obscured by noise. An attempt was made to employ global ocean model results (on a coarser grid than is available for the Pacific propagation database) to drive the Arena Cove FM; the results were unsatisfactory and will not be presented. When a better resolved global solution is available, this event may be added to the suite employed for forecast model testing since it should shed light on the extent to which bathymetric resolution may impact arrival time accuracy.

The sequence begins with a cautionary tale: the "tsunami-earthquake" induced Sanriku-1896 event. This was modeled by a suitably positioned unit source (KISZ-B25) with the slip appropriate to the reported Mw=7.6 magnitude. As shown, such an event would be expected to generate only a few centimeter signal at Arena Cove. Large run-ups, one meter in the case of the nearby town of Mendocino, occurred illustrating the fact that direct observation of deep-water waves is needed for realistic forecasting. The depth and frequency of sea floor motion for this event was such that the earthquake magnitude poorly indicated its devastating tsunami-generating potential to Japan's Sanriku coast.

Next consider the set of events from 1946-1964 that were felt in or near Arena Cove, though a tide gage had not yet been installed and the DART® array was still in the future (Unimak-1946 and Alaska-1964 were shown earlier.) In each case the source was represented by a weighted group of unit sources from the propagation database, or constructed to match source characteristics appearing in the literature (see Table 1 and Tang et al., 2006).

A number of other events between 1994 (East Kuril) and 2003 (Rat Island), listed in Table 1 and illustrated in Figures 21 and 22, generated weak responses in Arena Cove. In the case of East Kuril-1994, although the match is quite good, the presence of substantial noise in the tide gage record in advance of the waves' arrival, suggests a limitation on the detection of weak tsunami signals. Particularly in the winter months the tide gage record

DRAFT

at Arena Cove can be extremely noisy. This is true for the IrianJaya-1996 event; for Chile-1995 and Kuril-1995 the tide gage records are not readily available though they may be digitized in the course of an NGDC project. For the Andreanof-1996 event the model seems to capture the timing and periodicity of the Arena Cove response as it does perhaps for the Rat Island-2003 event. For the Peru-2001 and Hokkaido-2003 the match is less convincing. The Rat Island event is notable in the history of tsunami forecasting and the DART® array. Based on data from early elements of the DART® array of the Aleutian Islands, and without the conveniences of the SIFT system for "inversion", an estimate for the likely impact on the Hawaiian Islands (Titov et al. 2005) demonstrated the utility of direct sea level observation in tsunami forecasting.

The next set of Pacific basin historical events, depicted in Figure 23, are those between Tonga-2006 and Peru-2007. Excluded from the set is the Kuril event of November 15, 2006, that was examined earlier. That event, which was observed at several DART® sites, has become a classic for the NCTR modeling group. Tonga-2006 is reported in the NGDC database as producing a 27cm run-up at Crescent City but unfortunately only 6-minute sampled tide gage data are available at Arena Cove. Though the arrival time and first wave shape correspond reasonably well, the amplitude of the observations is considerably less that the model predicts. For Kuril-2006 the tsunami-capable instrument, with its 1-minute sampling, was in place and the early waves of the event were well represented by the forecast model. The same is true of Kuril-2007 which also played an important role in the development of the SIFT forecast tool. Unlike most preceding events whose source mechanism is a reverse thrust fault sending a leading peak toward the offshore DART® sites, this was a "normal" thrust event from which a leading trough propagated. As seen in Figure 23, this observed time series at Arena Cove is well matched by the model.

For the Solomon-2007 event the observations were weak and intermittent, though the amplitude of the model signal and its inclusion of larger late waves seems consonant with the data. Also shown in Figure 23, the Peru-2007 event was only weakly felt at Arena Cove and one might be tempted to view the observations as noise. If however the model result is shifted to the right by about ten minutes there is suggestion that the early event history is mimicked. Waves traveling from South America to the U.S. west coast occasionally arrive later than the propagation model predicts, perhaps due to the model bathymetry being smoother than the real ocean. Tsunami waves travel slower in shallower water and in consequence real waves may be delayed in passing through rugged ocean regions such as the Galapagos. Similar delays have been encountered in other forecasts and it remains to be seen whether, as more accurate bathymetric data become available, arrival time forecasts will improve. It should be emphasized that as a percentage of the overall travel time these delays are quite minor.

Late in the same year another event, Chile-2007, occurred off South America. The Arena Cove response, shown in Figure 24, was quite weak and difficult to match with model prediction. Two events from early 2009 are available for study. The predicted signal from the first, near Bird's Head in Papua-New Guinea, arrived at a noisy period at the Arena Cove tide gage and little if anything can be gleaned from the comparison. Two weeks

DRAFT

later an event of similar magnitude occurred off the Kuril Islands where tsunami waves impacting the west coast frequently originate. As seen in the lower right panel of Figure 24, the Arena Cove FM is reasonably successful in representing that response. Discussion of the Vanuatu 2009 is to be found below.

We now arrive at the events that are most recent at the time this report was written. The Samoa-2009 event was the most damaging to U.S. territory in recent years and, although the DART® array performed well in providing data to provide an accurate forecast, the proximity of the source to U.S. and Western Samoa did not permit any lead time there. This was a sizeable event and, even as far away as Arena Cove, a run-up of 44cm was reported. As seen in Figure 25 the Arena Cove FM performs very well in replicating the early waves, though the later waves may be underestimated. This is an instance in which the reference model (see Figure 18) may, in light of the substantial lead-time inherent in such remote source situations, be a worthwhile option. With a workstation-level computer, the run-time of the FM is presently about 10 hours of clock time for 8 hours of simulation. With advances in computing power or the migration of operational computing to supercomputers it may be possible to depart from the current standard of about 10 minutes per 4-hours of simulation with a FM, perhaps even to run the basin-wide solution in real time with enhanced resolution. Just days after the Samoa-2009 event, another occurred off Vanuatu. Though much less damaging, this event had a new feature to exercise the tsunami community. Vanuatu-2009 was a composite event with two earthquakes in a 15-minute period. Though not yet part of the standard set of historic events for FM evaluation, the separate source characterizations have been established at NCTR (Wei, personal communication). Blending the two forcing histories with an appropriate time delay provides the input needed for a FM (or RM) and the result for the mild response at Arena Cove is quite gratifying. The final historical event analyzed for the first draft of this report is associated with the major earthquake that struck Chile on February 27, 2010. Causing major damage and loss of life locally the tsunami waves propagated widely throughout the Pacific. The waves, seen at DART® 32412, provided a good estimate of the remote hazard, particularly to Hawaii, indicating that wide scale evacuation was not necessary. On the U.S. west coast, noticeable tsunami effects were observed matching predictions. At Arena Cove, had this model been then available and included in the SIFT system, it would have been another point of success for the forecast system in the emergency response to Chile-2010. As seen in Figure 25, there is very close agreement between the FM hind cast and tide gage observation. During the internal NCTR review of this report the Honshu region of Japan was struck, on March 11, 2011, by a huge earthquake, generating a tsunami that caused local devastation and serious impacts throughout the Pacific basin. The FM for Arena Cove was employed in real-time and the results are described briefly in subsection 4.6.

To summarize the analysis of historical events, given above and in subsection 4.6, it would appear that the Arena Cove FM is capable of producing accurate forecasts for this open coast site on the U.S. west coast. Though the observed waves may be difficult to observe accurately at the tide gage during winter storms, the objective of producing credible forecasts of tsunami impact appears to have been met.

DRAFT

4.5 The Mendocino Earthquake of April 25, 1992

Of special interest to northern California is the Mendocino earthquake of April 25, 1992. This has the distinction of being the most recent substantial thrust event on the Cascadia subduction zone. While strike-slip events are commonplace offshore in this region, as shown in Figure 26, it is thrust faults that have the potential to generate significant vertical displacements of the sea floor that cause large tsunamis. The epicenter of this event was on land to the southeast of the plate triple-junction off Cape Mendocino. Uplift of the order of a meter of a 25km stretch of the nearshore, between Cape Mendocino and Punta Gorda to the south was evident in a die-off of intertidal organisms as reported by Carver et al., (1994). Presumably extending offshore too, this deformation is not well represented well by either of the southernmost unit sources (ACSZ-A/B65) now available in the propagation database. The model predictions based on either of these unit sources with an appropriate scale factor for the magnitude 7.2 event underestimate the tide gage signal at Arena Cove, as seen in Figure 26. Another feature of interest of this event, described by Gonzålez et al. (1995) is that its proximity to shore may have generated a train of coastal-trapped edge waves. Traveling slower than normal tsunami waves taking a deep-water route, the edge waves may have extended the duration of the event at nearby locations to the north and south. This possibility, and the suggestion that the ACSZ source line ought to be extended at least one unit further south, make this an event worth further study. The reference and forecast models for Arena Cove and others existing or planned for the west coast (Eureka, Crescent City, etc.) have a major role in ongoing risk assessment studies for Cascadia.

4.6 The Honshu Tsunami of March 11, 2011

During the NCTR internal review of this report, the severe earthquake and consequent tsunami occurred off the east coast of Honshu, Japan. The SIFT forecast system, ingesting timely data from nearby DART® sites, performed well and provided the basis for appropriate response at those sites for which forecast models were available. Among these was Arena Cove, CA and it seems appropriate to add Honshu-2011 to the suite of historical events for which observations, and both forecast model and reference model results, are available.

The results are shown in Figure 27 where, in the upper panel, the RM and FM time series at the Arena Cove tide gage (drawn as black and red lines respectively) are compared with the 1-minute tide gage record (in blue.) While the largest tsunami waves fortuitously arrived near low water for the U.S. West Coast, and the NCTR models employ mean high water (MHW) in order to represent "worst case" conditions, the agreement is excellent. As at other sites, there was a slight discrepancy in the arrival time (9 minutes in the case of Arena Cove) that has been compensated for in Figure 27. This error is less than 1.6% of the overall travel time and is believed to be associated with the relatively coarse grid of the propagation database which provides the boundary conditions of the finer scale nested FM and RM grids.

DRAFT

After the first few waves the timing and amplitude of the crests and troughs lose synchronicity, both between the RM and FM and between these and the observations. Nonetheless the character of the response it well replicated and the maximum runup agrees well with the reported 1.55m provided by the NGDC database. The latter is the difference between actual and predicted sea level and suggests that, in the case of Arena Cove itself, the forecast wave height is not overly sensitive to the state of the tide, though the extent of inundation may be overstated.

The second row of Figure 27 contrasts the RM and FM solutions at a time, indicated by the green line in the upper panel, where the solutions have begun to diverge. It illustrates that both wave amplitude and tsunami-induced currents are in good agreement through most of the region shown. As before there is some discrepancy near shore at the northern and southern limits of the FM C-grid and near the complex topography off Point Arena Light. The lower panels of the figure contrast the RM and FM predictions for maximum wave amplitude. No reports of amplitude or inundation are available for comparison with these predictions but the agreement would appear to be best near shore for this event. In particular the maxima predicted for Arena Cove and the inundation near the mouth of the Garcia River and much of Manchester Beach match well. If there is error, the FM appears to err on the conservative side, overstating the likely impact.

4.7 Simulation of the remaining Synthetic Mega-events

We conclude this section with a summary of other model runs that were made in order to verify its stability, but which provide useful information on the exposure of Arena Cove to potentially hazardous future events within the Pacific. As noted earlier, the sparse instrumental record of actual events needs to be augmented with credible scenarios to permit risk assessment. While not pretending to be a full-blown risk assessment for the Arena Cove - Manchester Beach area, the full set of mega-tsunamis modeled during stability testing can provide some early estimates.

Results for the set of 19 mega-tsunamis, based on the FM are presented in Figure 28. At the center of each source zone (1000x100km in extent, with the long axis aligned with the local plate boundary and a uniform slip distribution corresponding to an event magnitude of 9.3) a color-coded square represents the impact at Arena Cove. The measure of impact employed is the maximum amplitude of the predicted time series at the reference point (for the Arena Cove FM, the tide gage location near the head of the pier.) There is not any simple relationship between source orientation, location, or great circle distance to Arena Cove; focusing associated with seafloor features can more than compensate for the decay associated with geometric spreading. In Figure 29, FM prediction of the inundation that might result from some of these scenarios are drawn together with (in the lower right panel) an ensemble representing the selection employed in the CalEMA study, whose inundation line is drawn in red.

DRAFT

5.0 Conclusions

In conclusion, good agreement between observations and model predictions for a subset of historical events, including the recent Honshu-2011 tsunami, has been established and the stability of the model for numerous synthetic events has been demonstrated. In particular the reliability of the forecast model, designed to run rapidly in a real time emergency conditions, has been proven by the favorable comparison with reference model predictions, particularly during the early hours of an event. The model will be included in the SIFT system employed operationally at the Tsunami Warning Centers, and will permit the Point Arena – Manchester area to be added to the coastal communities for which forecast capability is available. Additionaly it provides a tool of use in risk assessment for the Arena Cove area.

In addition to the scenarios run by the author, and reported here, further tests have been made by other members of the group at NCTR, and will continue to be made by staff at the Warning Centers and others, perhaps in training situations. Among the many related tools developed at NCTR is ComMIT (Community Model Interface for Tsunami, nctr.pmel.noaa.gov/ComMIT/), which provides a highly intuitive graphical environment in which to exercise and explore forecast models for any combination of propagation database unit sources. Were any of these avenues to reveal a problem with the model, its origin (most likely in some quirk of the bathymetric files) would be located and corrected then the revised version re-installed for operational use. The development of the forecast system will be a dynamic process, with new models added (and old ones revisited) from the current list of U.S interests and globally. In the coming years it is expected that further capabilities (for example landslides) will be added as algorithms and methodologies mature.

6. Acknowledgments

Many members of the NCTR GROUP provided valuable assistance in the production of this report. In particular Nicolas Arcos edited the first draft for content and style. CalEMA and other California entities distribute GIS online dataset used in the graphics. The modeling could not proceed without the detailed DEM produced at NGDC by the painstaking combination of numerous bathymetric and topographic surveys. Imagery used in the earlier figures has been reproduced with permission from the California Coastal Records Project (www.californiacoastline.org) and the Mendocino County Historical Society. This publication is [partially] funded by the Joint Institute for the Study of the Atmosphere and Ocean (JISAO) under NOAA Cooperative Agreements NA17RJ1232 and NA10OAR4320148, Contribution No. XXXX. It is PMEL Contribution No. NNNN

DRAFT

7. References

Arcas, D. and B. Uslu (2009): PMEL Tsunami Forecast Series: Vol. 2. A Tsunami Forecast Model for Crescent City, California

Barberopoulou, A., J. C. Borrero, B. Uslu, M. R. Legg and C. E. Synolakis (2011): A Second Generation of Tsunami Inundation Maps for the State of California. Pure and Appl Geophys.

Barberopoulou, A., J. C. Borrero, B. Uslu, N. Kallogeris, J. D. Goltz, R. I. Wilson, and C.E. Synolakis (2009): New Maps of California to Improve Tsunami Preparedness. *Eos, Trans. AGU, Vol.90, No.16, 21 April 2009*. See: www.conservation.ca.gov/cgs/geologic_hazards/Tsunami/Inundation_Maps/

Carver, G.A., A.S. Jayko, D.W. Valentine and W.H. Li (1994): Coastal uplift associated with the 1992 Cape Mendocino earthquake, northern California. Geology 22(3), 195-198.

Driscoll, N.W., Weissel, J.K., and Goff, J.A., 2000, Potential for large-scale submarine slope failure and tsunami generation along the US mid-Atlantic Coast (pdf). *Geology 28*, (5), 407-410.

Dudley, W.C. and Min Lee (1998): Tsunami! University of Hawai'i Press, 362pp.

Dunbar, P. (2007): Increasing public awareness of natural hazards via the Internet. Nat. Hazards 42(3) 529-536, DOI: 10.1007/s11069-006-9072-3

Fine, I.V., A.B. Rabinovich, B.D. Bornhold, R.E. Thomson, and E.A. Kulikov (2005): The Grand Banks landslide-generated tsunami of November 18, 1929: preliminary analysis and numerical modeling. *Marine Geology 215*, 45–57.

Friday, D.Z., L.A. Taylor, B.W. Eakins, R.R. Warnken, K.S. Carignan, R.J. Caldwell, E. Lim, and P.R. Medley: Digital Elevation Model of Arena Cove, California: Procedures, Data Sources and Analysis. www.ngdc.noaa.gov/mgg/inundation/tsunami/data/arena_cove_ca/arena_cove_ca.pdf

Gica, E., M. Spillane, V.V. Titov, C.D. Chamberlin, and J.C. Newman (2008): Development of the forecast propagation database for NOAA's Short-term Inundation Forecast for Tsunamis (SIFT). NOAA Tech. Memo. OAR PMEL-139, NTIS: PB2008-109391, 89 pp.

Gonzålez, F.I., K. Satake, E.F. Boss and H.O. Mofjeld (1995): Edge wave and non-trapped modes of the 25 April 1992 Cape Mendocino tsunami. Pure and Appl. Geophys. 144, 409-426, DOI: 10.1007/BF00874375

Haugan, J. (2005): Dog Holes And Wire Chutes. In: Maritime Life and Traditions, No.

DRAFT

29, Winter 2005.

Lander, J.F., and P.A. Lockridge (1989): United States Tsunamis, 1690 to 1988, Publ. 41–2. National Geophysical Data Center, Boulder, CO, 265 pp.

O'Brien, M.P. (1946): Preliminary Report on Seismic Sea Waves from Aleutian Earthquake of April 1, 1946, Tech. Rep. HE 116207, Wave Project, Fluid Mechanics Lab., U. Cal. (Berkeley).

Percival, D.B., D. Arcas, D.W. Denbo, M.C. Eble, E. Gica, H.O. Mofjeld, M.C. Spillane, L. Tang, and V.V. Titov (2009): Extracting tsunami source parameters via inversion of DART® buoy data. NOAA Tech. Memo. OAR PMEL-144, 22 pp.

Spillane, M.C., E. Gica, V.V. Titov, and H.O. Mofjeld (2008): Tsunameter network design for the U.S. DART® arrays in the Pacific and Atlantic Oceans. NOAA Tech. Memo. OAR PMEL-143, 165 pp.

Tang, L., C. Chamberlin, E. Tolkova, M. Spillane, V.V. Titov, E.N. Bernard, and H.O. Mofjeld (2006): Assessment of potential tsunami impact for Pearl Harbor, Hawaii. NOAA Tech. Memo. OAR PMEL-131, NTIS: PB2007-100617, 36 pp.

Tang, L., V.V. Titov, and C.D. Chamberlin (2009): Development, testing, and applications of site-specific tsunami inundation models for real-time forecasting. *J. Geophys. Res.*, *114*, C12025, doi: 10.1029/2009JC005476.

ten Brink, U.S., Lee, H.J., Geist, E.L., Twichell, D.C., (2009): Assessment of tsunami hazard to the U.S. East Coast using relationships between submarine landslides and earthquakes. *Mar. Geol. 264*, 65–73

Titov, V., and F.I. González (1997): Implementation and testing of the Method of Splitting Tsunami (MOST) model. NOAA Tech. Memo. ERL PMEL-112, NTIS: PB98-122773, NOAA/Pacific Marine Environmental Laboratory, Seattle, WA, 11 pp.

Titov, V.V., and C.E. Synolakis (1998): Numerical modeling of tidal wave run-up. *J. Waterw. Port Coast. Ocean Eng.*, *124*(4), 157–171.

Titov, V.V., F.I. González, E.N. Bernard, M.C. Eble, H.O. Mofjeld, J.C. Newman, and A.J. Venturato (2005): Real-time tsunami forecasting: Challenges and solutions. Nat. Hazards, 35(1), Special Issue, U.S. National Tsunami Hazard Mitigation Program, 41–58.

U.S. Secretary of War (1914): Harbor of Refuge at Point Arena, or Elsewhere on the Pacific Coast, Between San Francisco and Humboldt Bay, California. Report to 63rd Congress, House of Representatives, Washington D.C., Document No. 1369, 39pp.

DRAFT

Wei, Y., E. Bernard, L. Tang, R. Weiss, V. Titov, C. Moore, M. Spillane, M. Hopkins, and U. Kânoğlu (2008): Real-time experimental forecast of the Peruvian tsunami of August 2007 for U.S. coastlines. *Geophys. Res. Lett.*, *35*, L04609, doi: 10.1029/2007GL032250.

DRAFT

FIGURES

DRAFT

Figure 1. The Point Arena area of southern Mendocino County, CA.

Figure 2. Views of present-day Arena Cove and its appearance in the early 1900's.

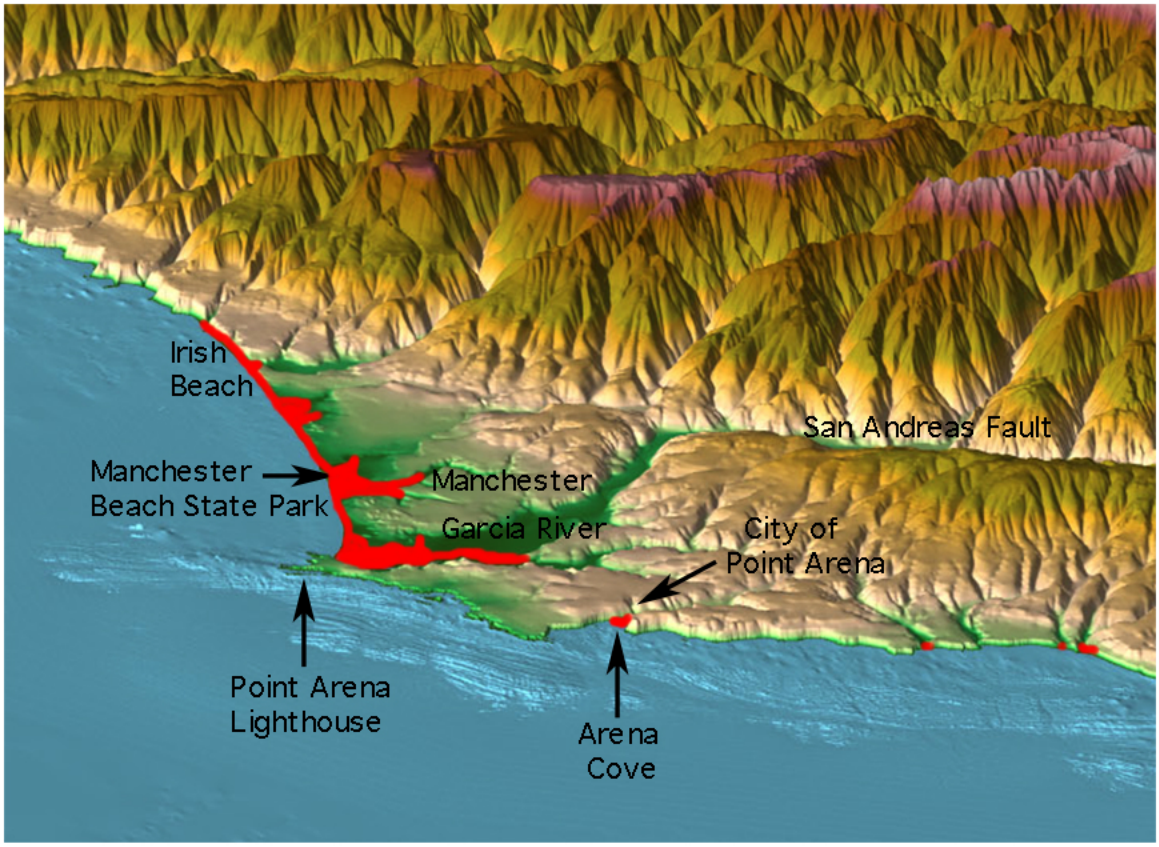

Figure 3. Extract from the oblique 3-D view of the Arena Cove DEM, provided by NGDC; sites of potential inundation identified by CalEMA are highlighted in red.

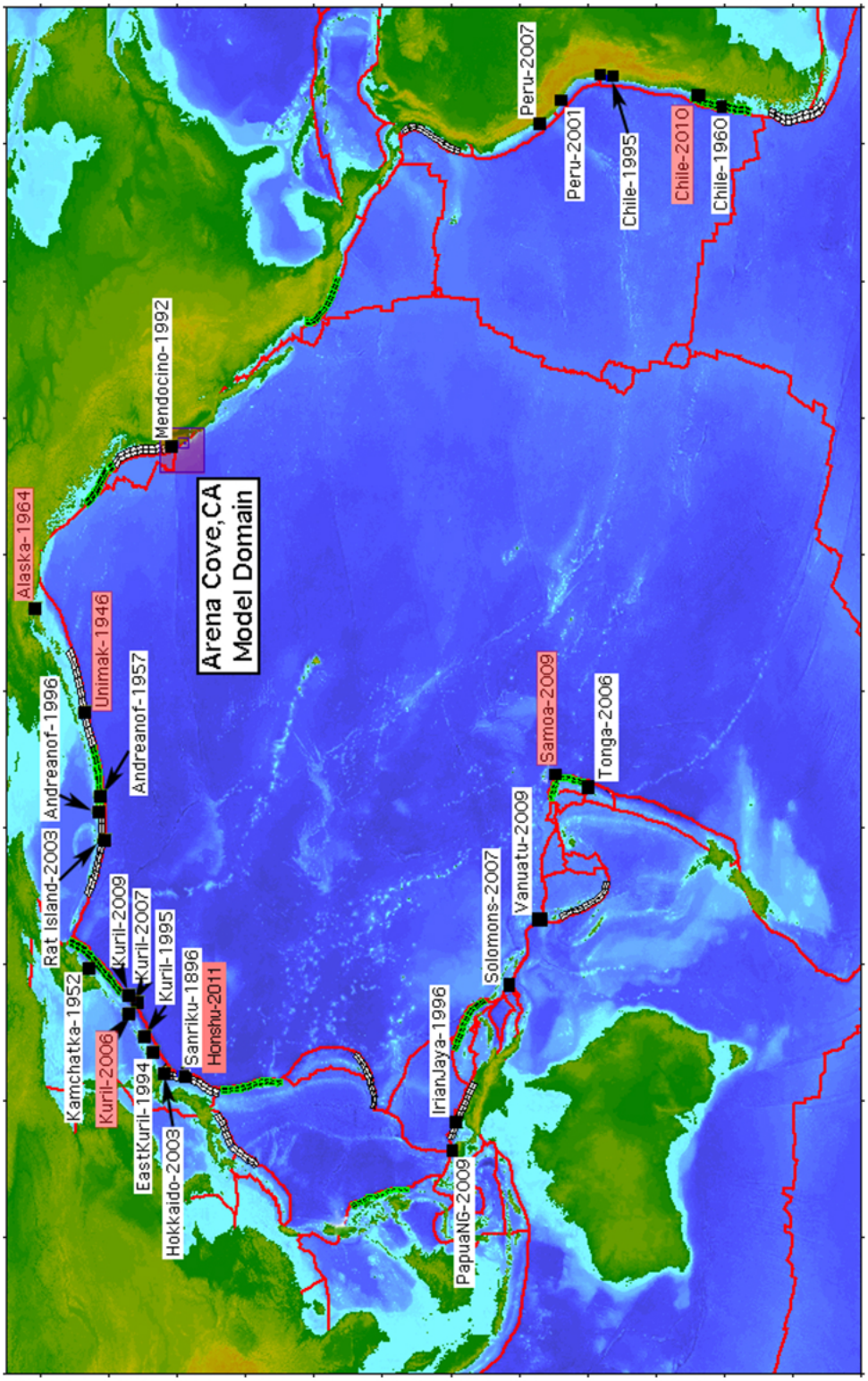

Figure 4. Distribution of the historical tsunami sources employed for the development of the Arena Cove forecast model. Those highlighted in red are more extensively investigated using the reference model.

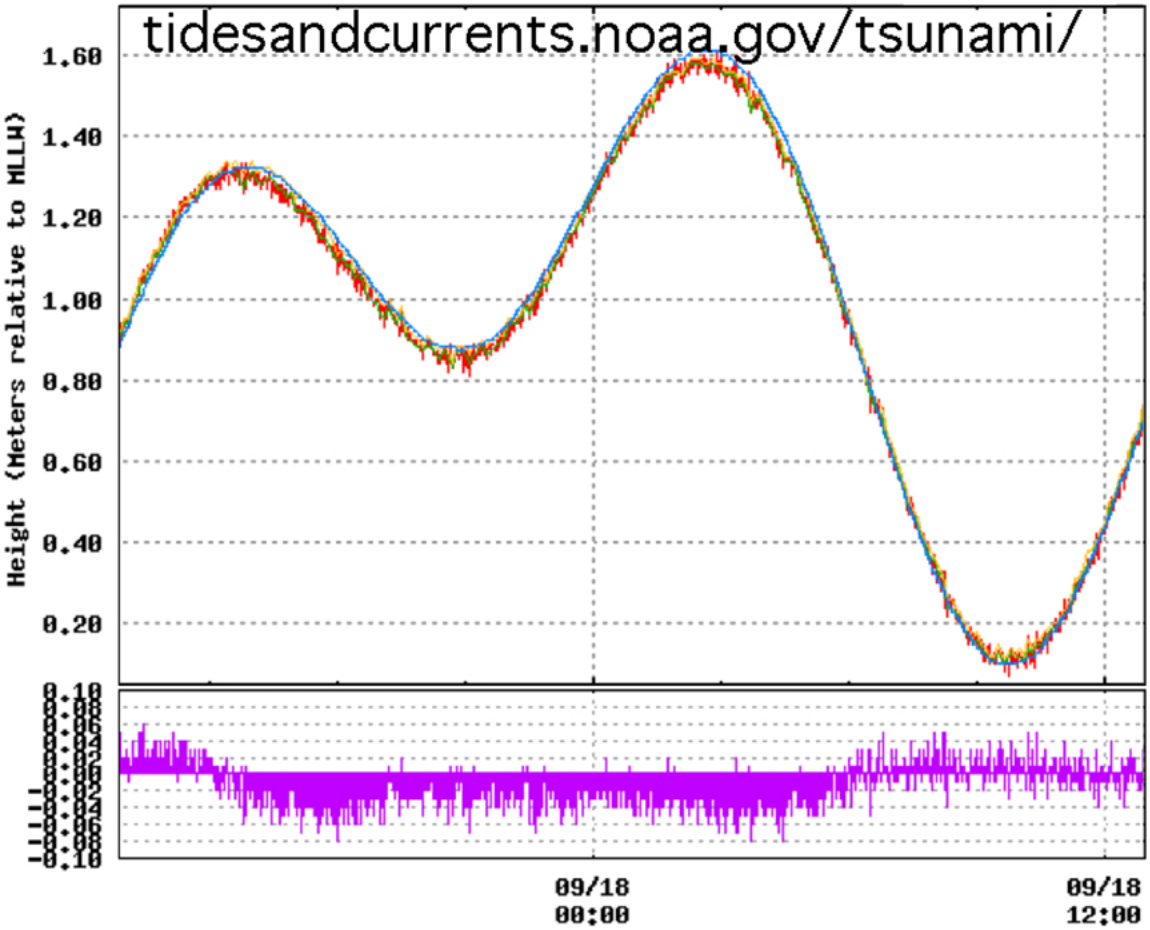

Figure 5. A sample interval from the Arena Cove tsunami-capable tide gage.

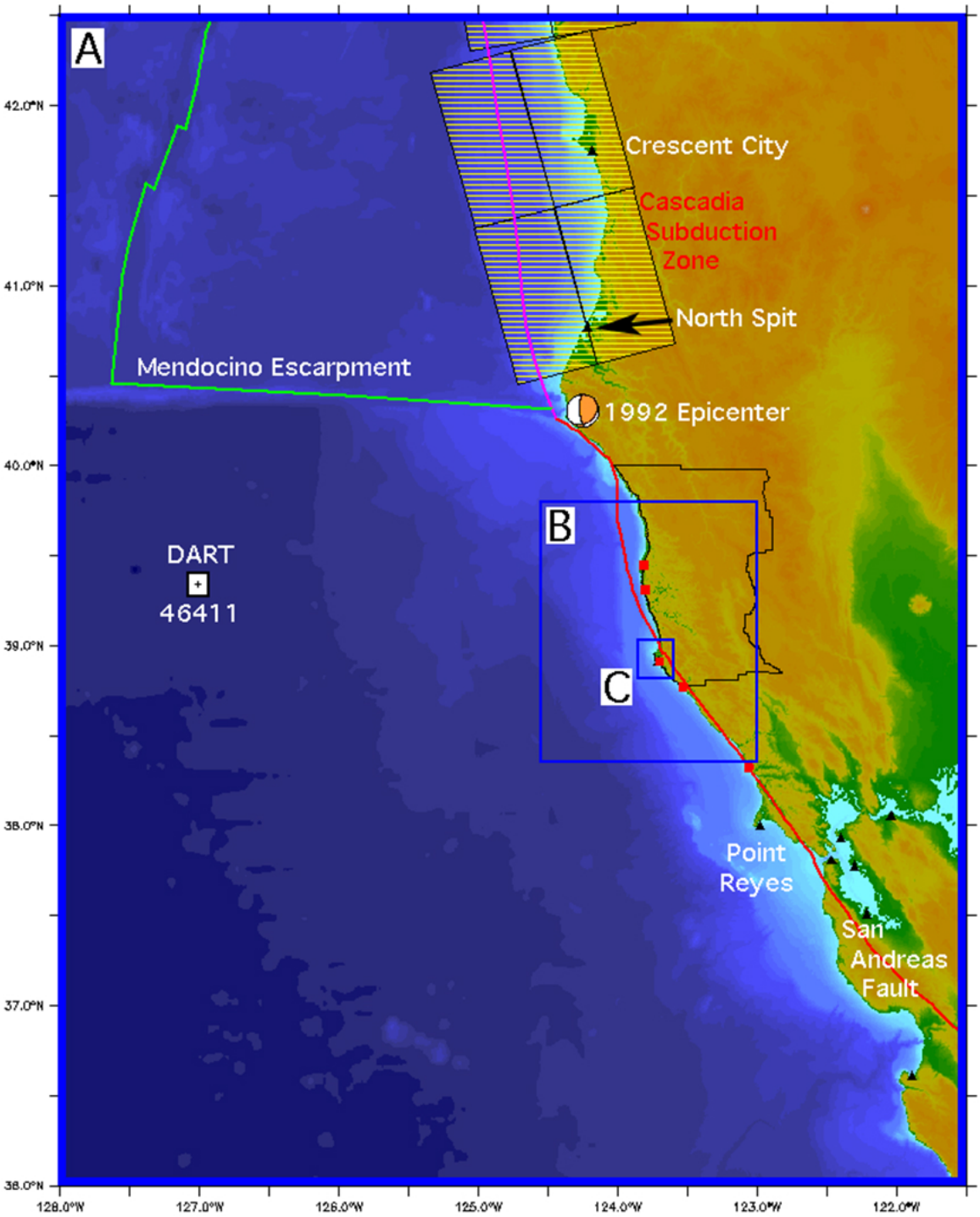

Figure 6. The setting of the Arena Cove model.

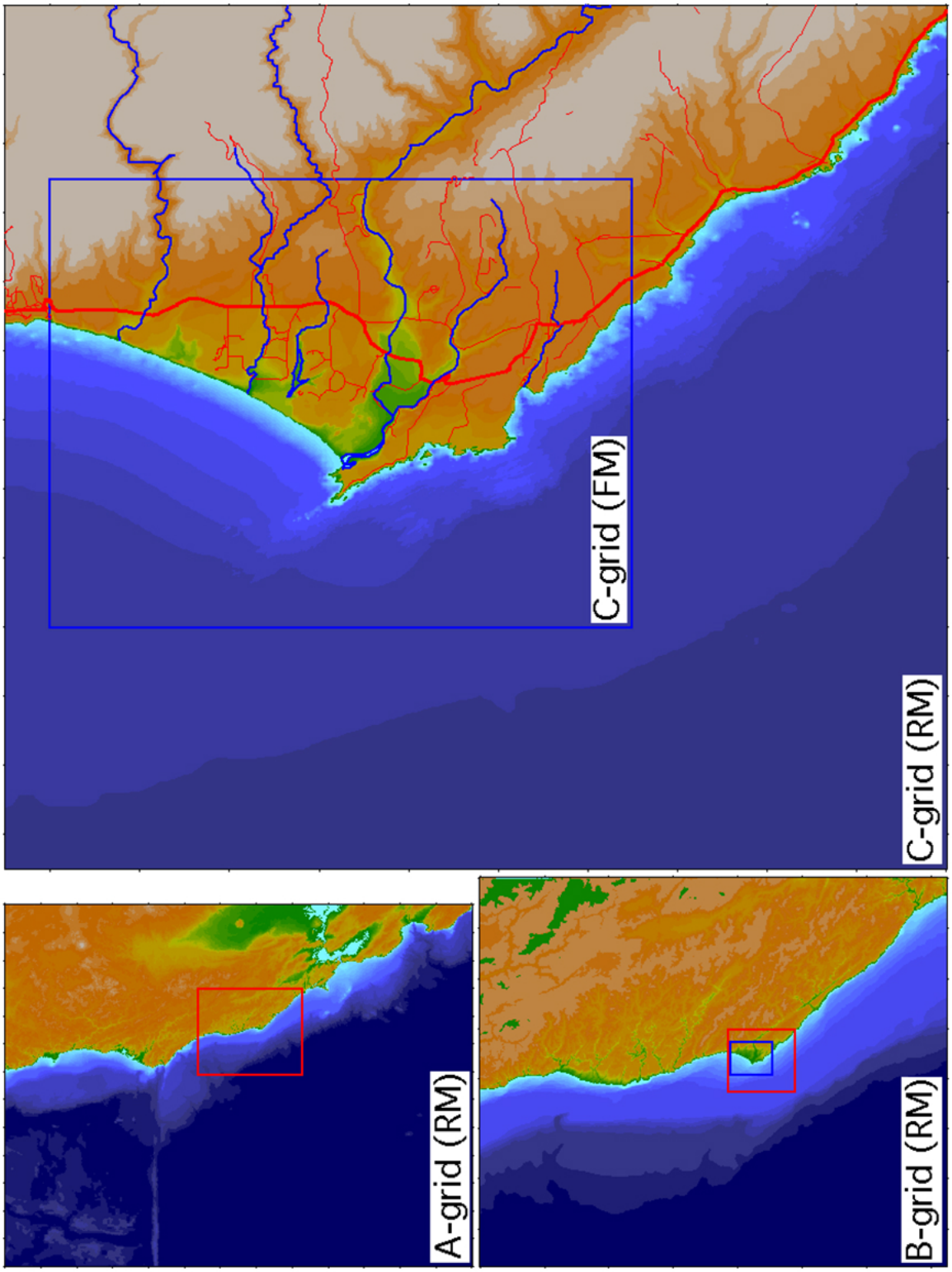

Figure 7. Nested grid representation for the Reference Model (RM). Rectangles are drawn, when appropriate, to indicate the placement of the next nesting level.

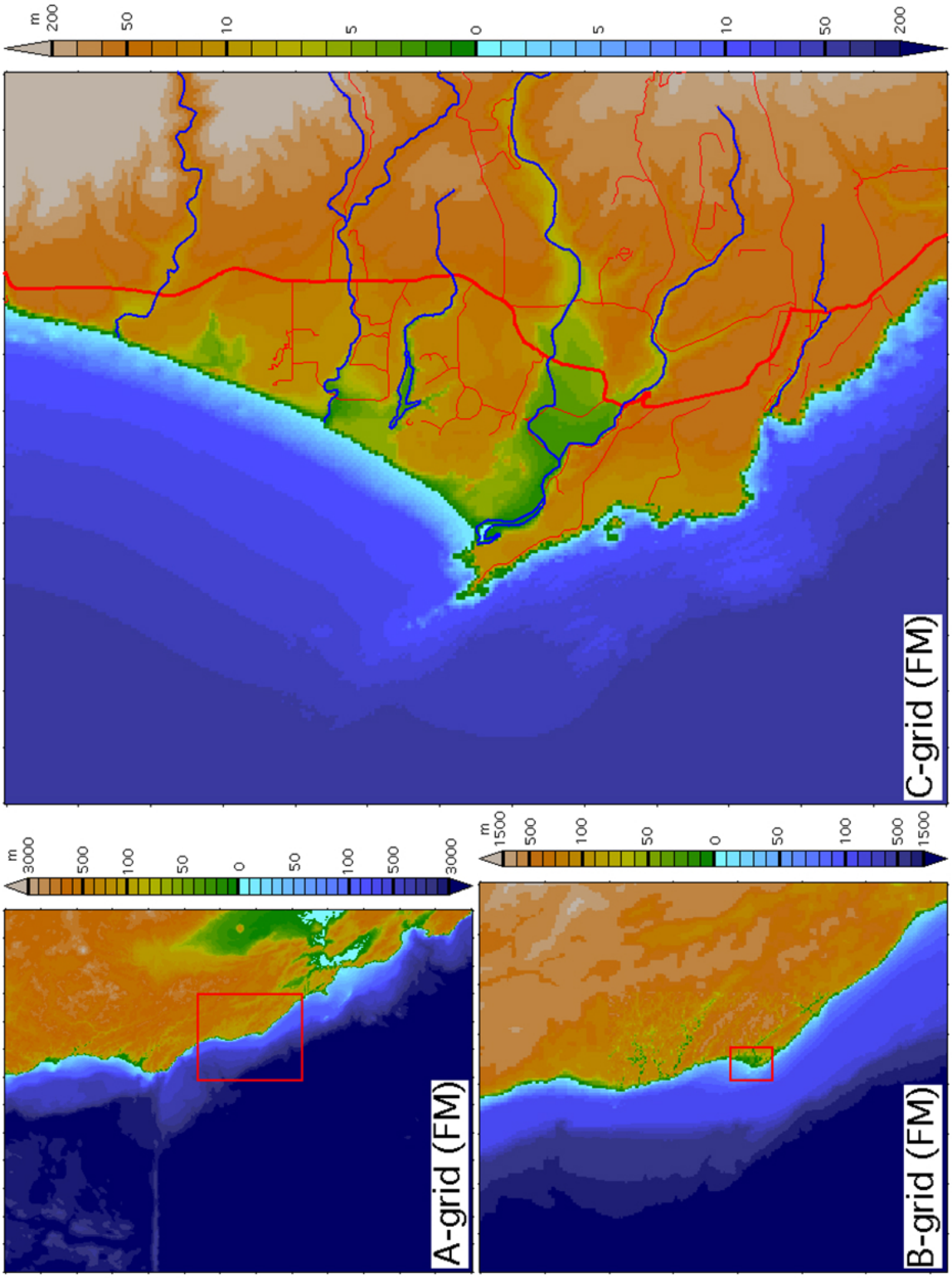

Figure 8. Nested grid representation for the Forecast Model (FM). Rectangles are drawn, when appropriate, to indicate the placement of the next nesting level.

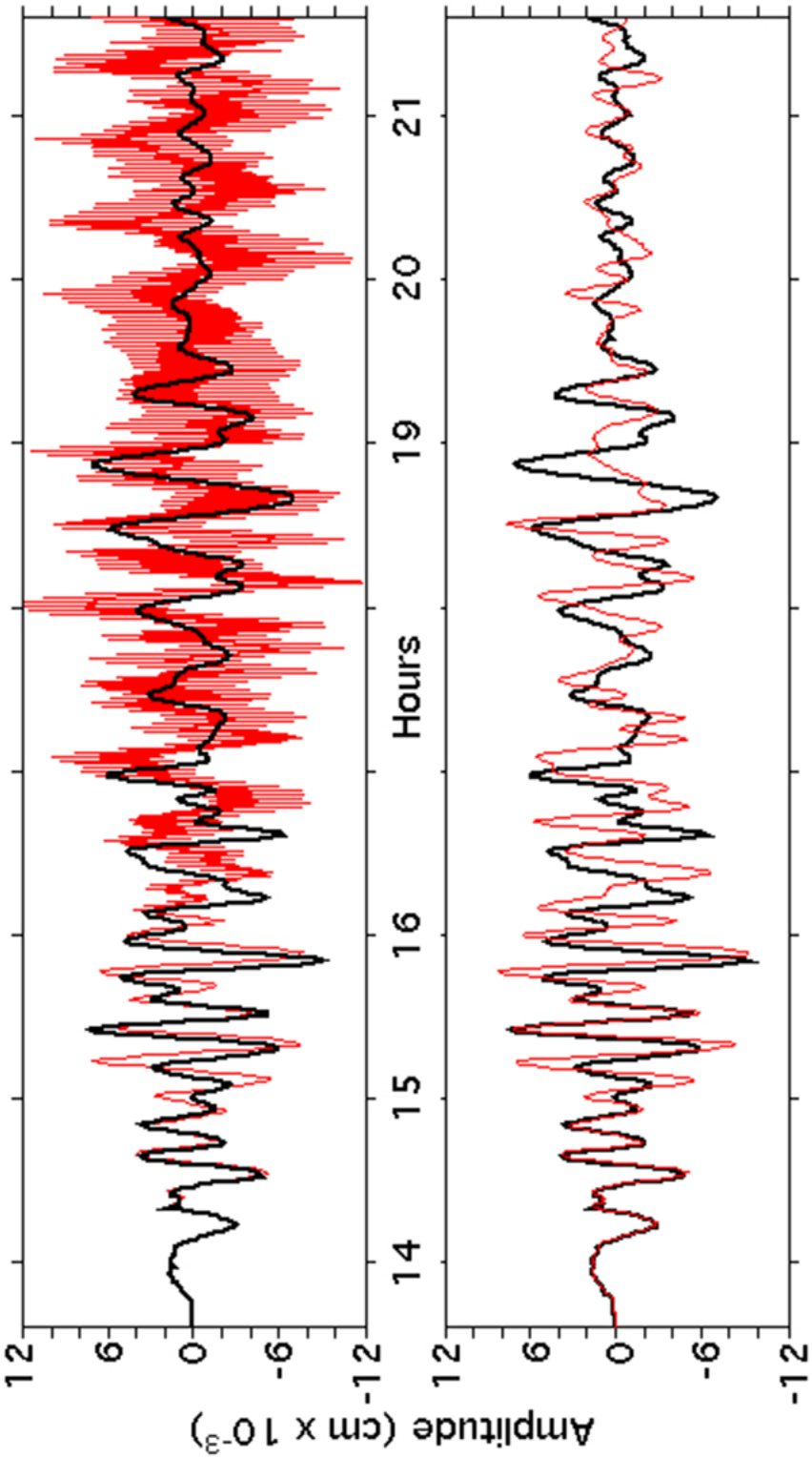

Figure 9. Illustration of the appearance of model instability (upper panel.) The RM C-grid bathymetry in this case required minor modifications, following which the “null” test gave satisfactory results.

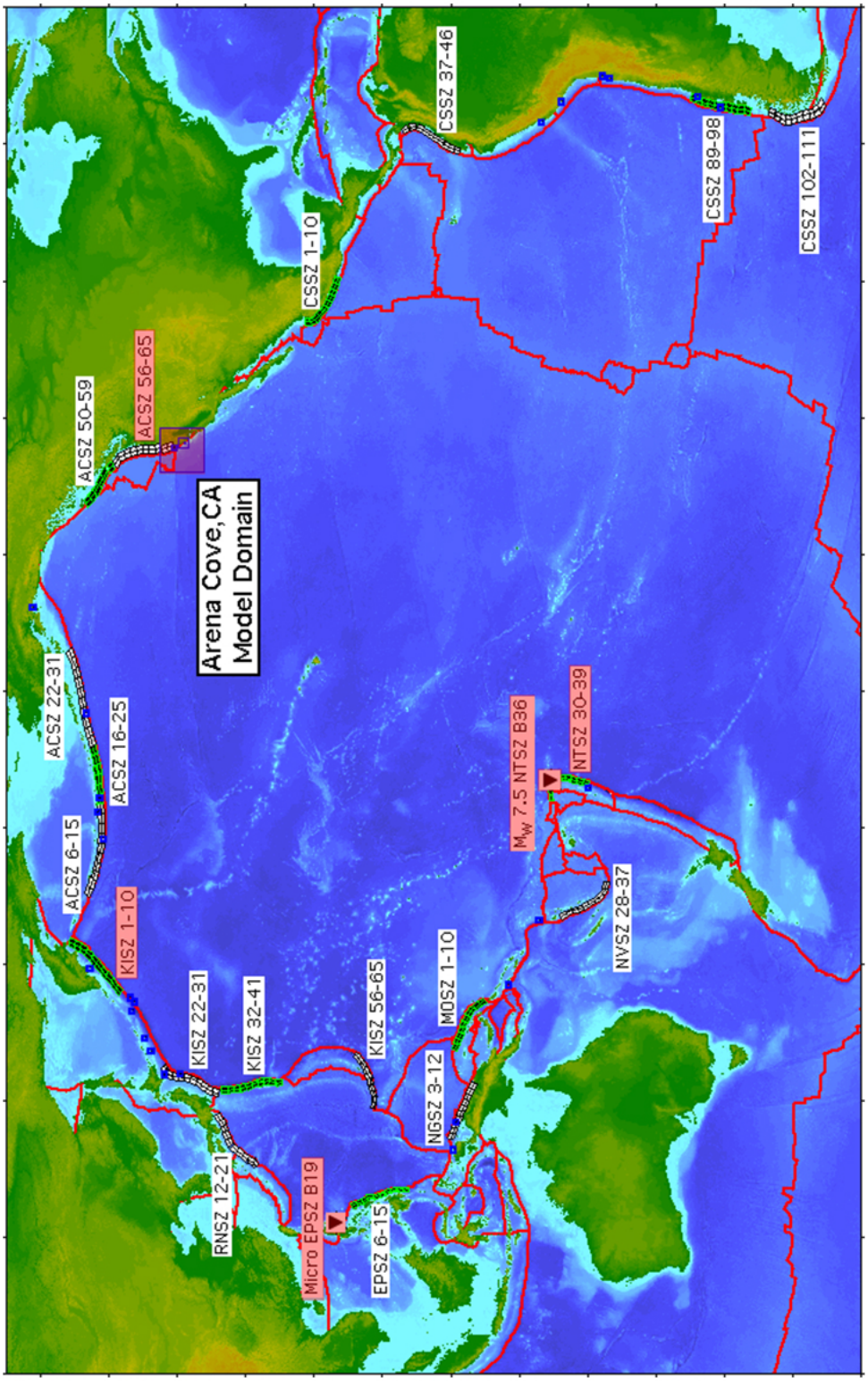

Figure 10. Locations of synthetic tsunami scenarios employed in model development.

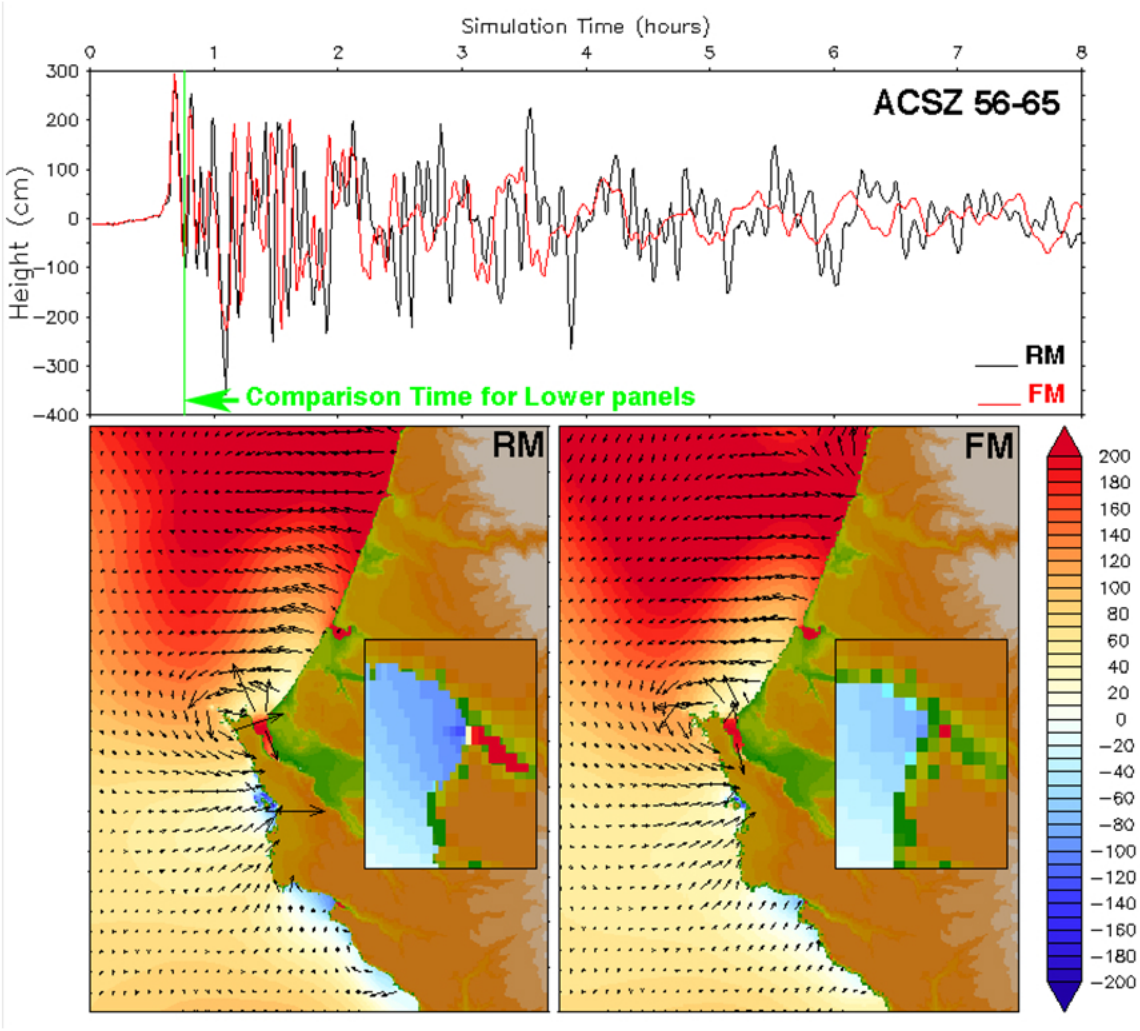

Figure 11. Comparison of Reference (RM) and Forecast (FM) model results for the ACSZ 56-65 synthetic mega-event, representing the Cascadia Subduction Zone. Time series at the tide gage location in Arena Cove are shown in the upper panel. The lower panels contrast the RM and FM amplitude and velocity fields at the time indicated. Insets are enlargements of Arena Cove.

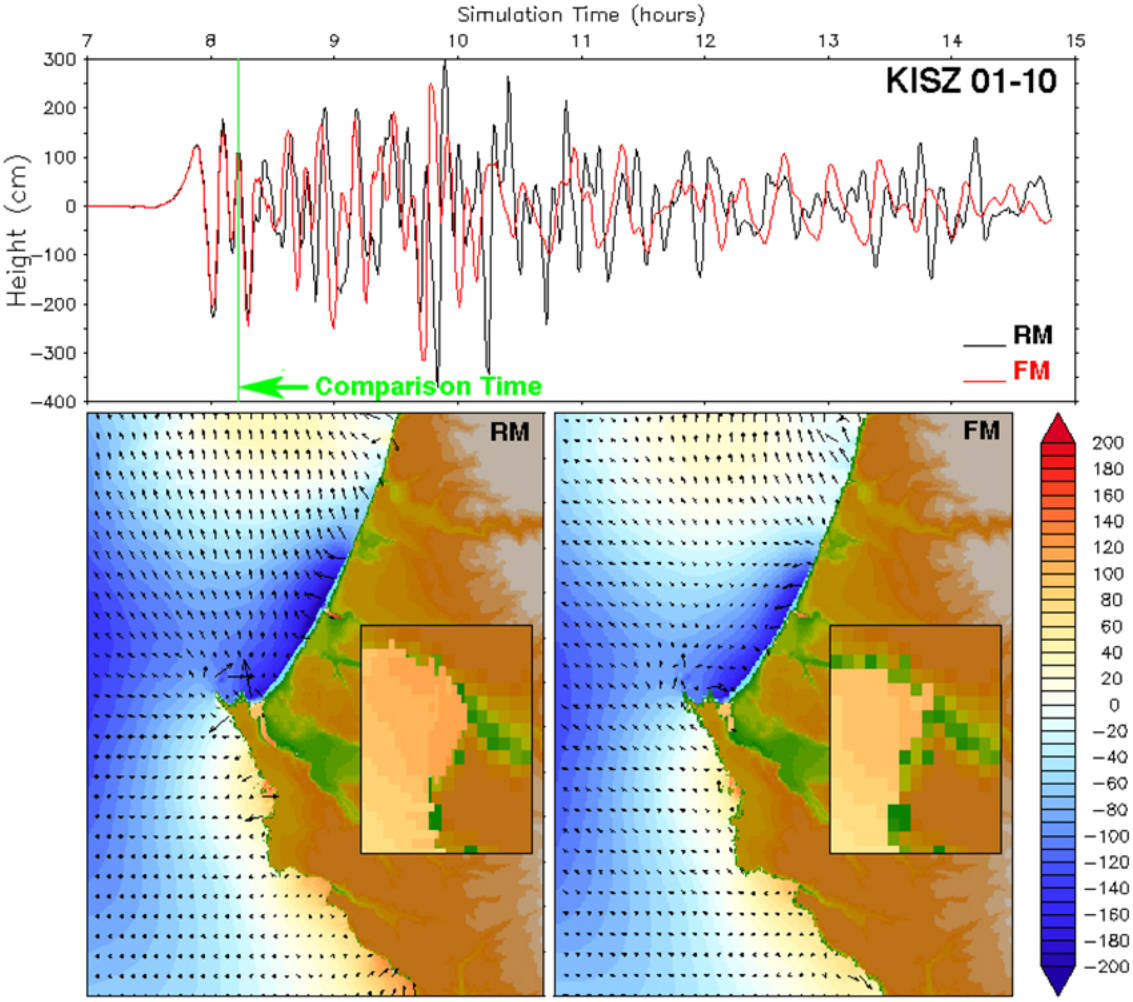

Figure 12. As in Figure 11, but for the KISZ 01-10 scenario representing Kamchatka.

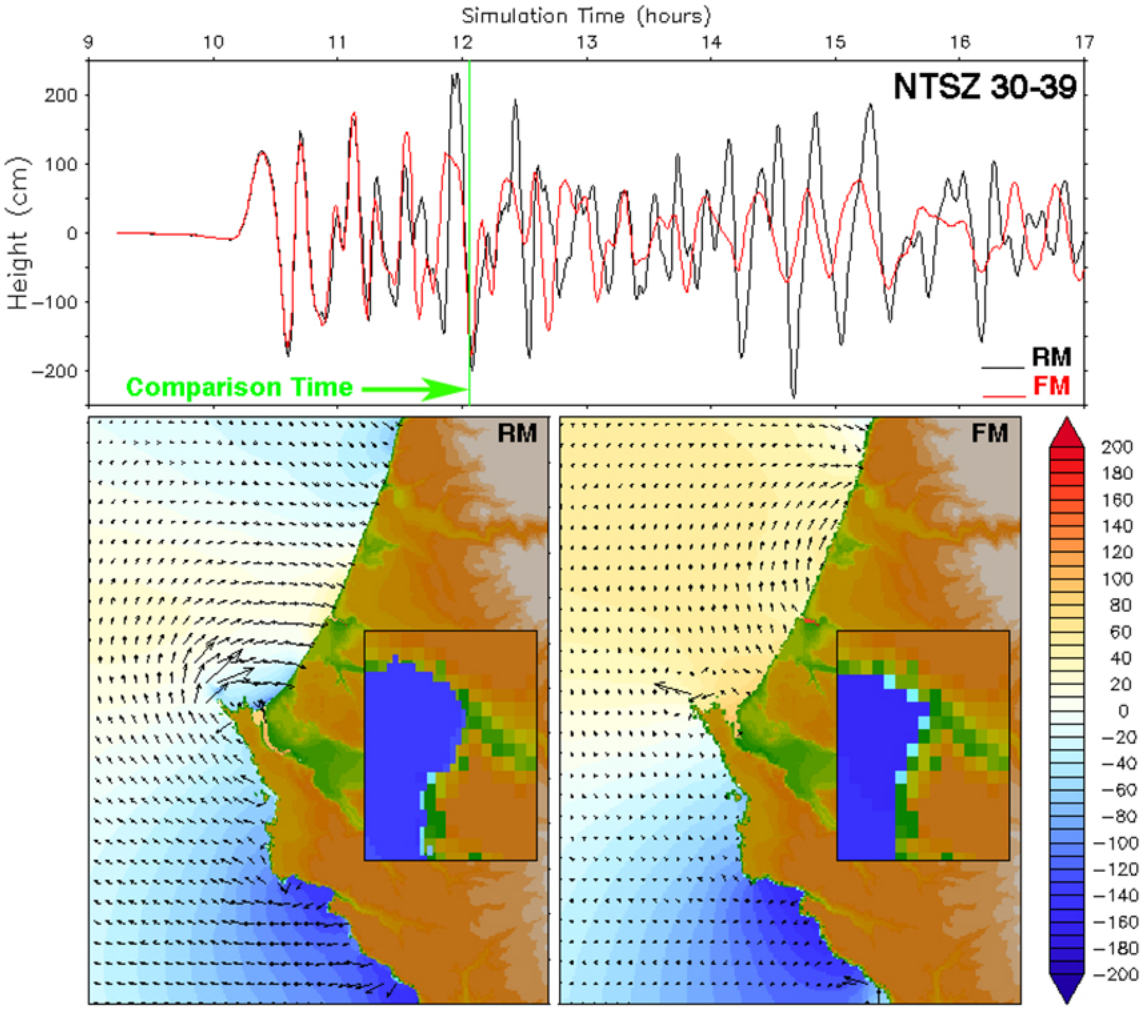

Figure 13. As in Figure 11, but for the NTSZ 30-30 scenario representing Samoa.

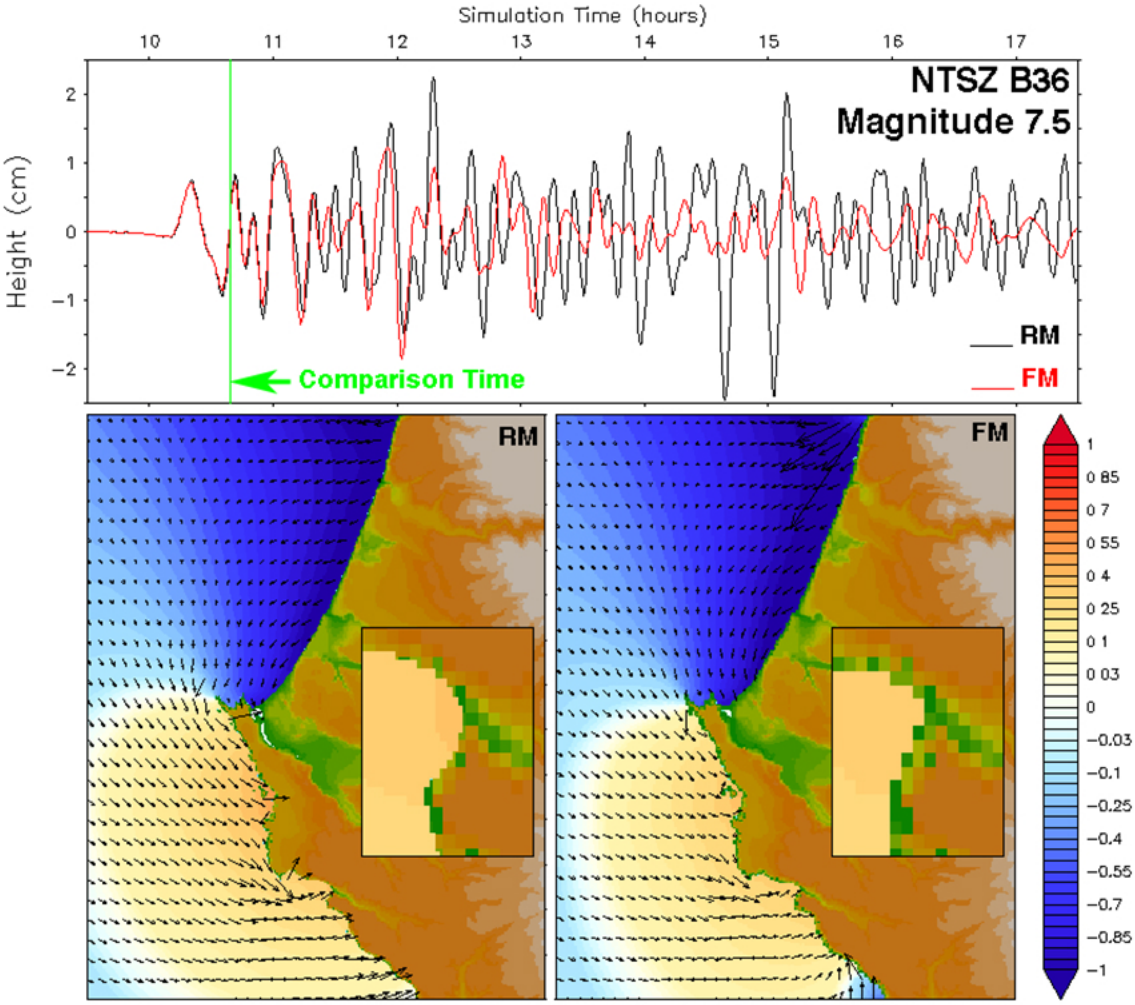

Figure 14. Comparison of the Reference and Forecast Model response to a synthetic moderate event at NTSZ B36 near Samoa.

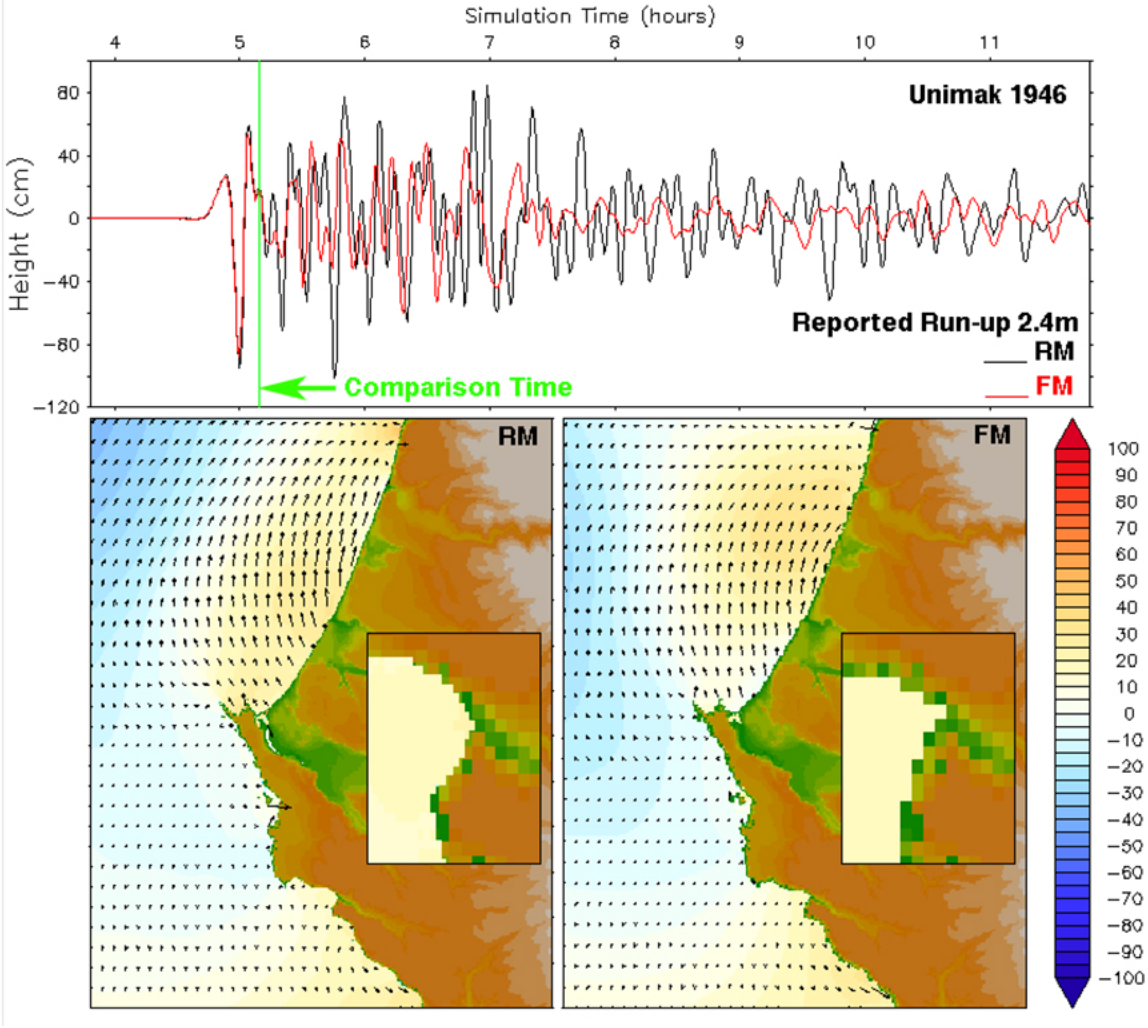

Figure 15. Comparison of the RM and FM response for the historical Unimak-1946 tsunami (prior to Arena Cove tide gage).

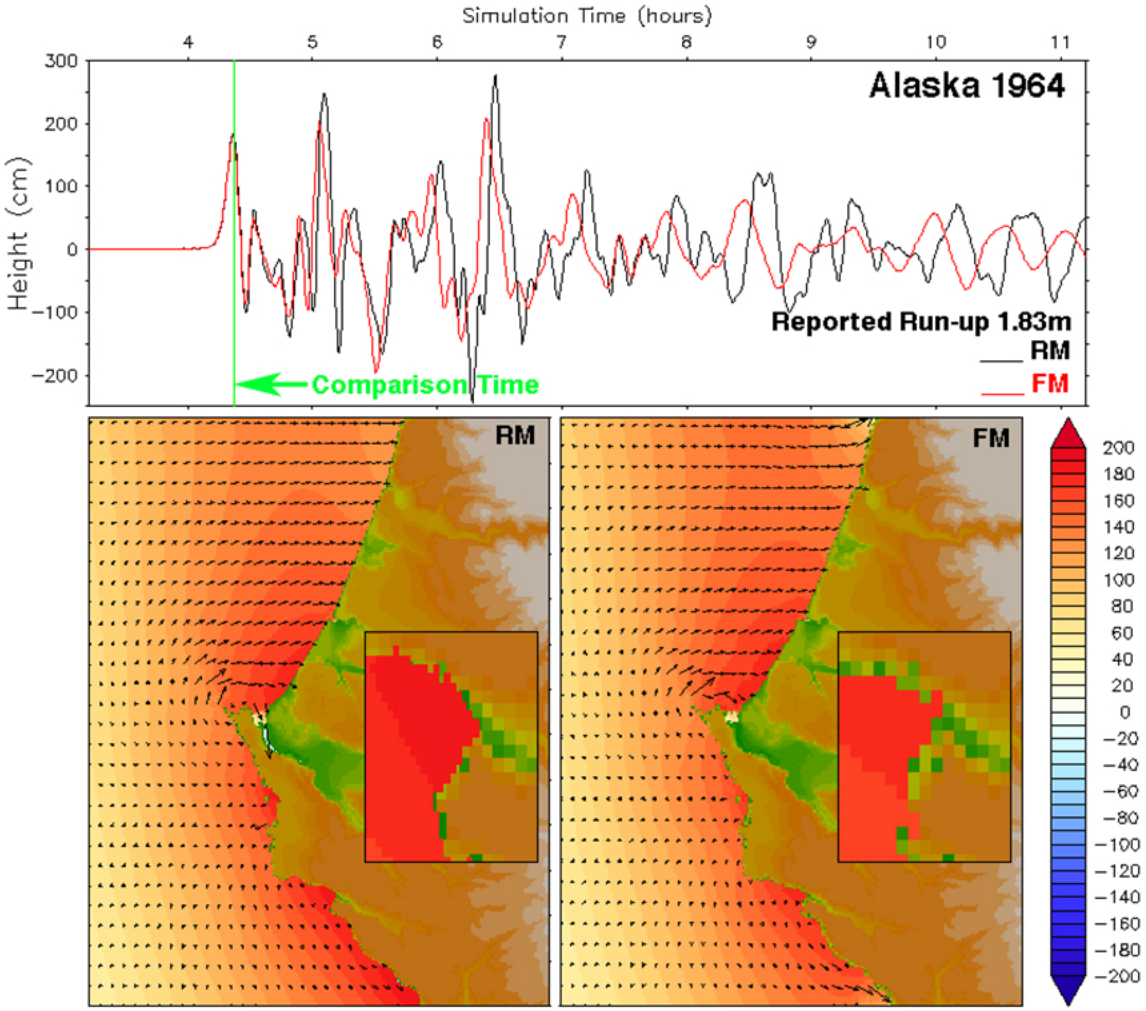

Figure 16. Comparison of the RM and FM response for the historical Alaska-1964 tsunamis (prior to Arena Cove tide gage).

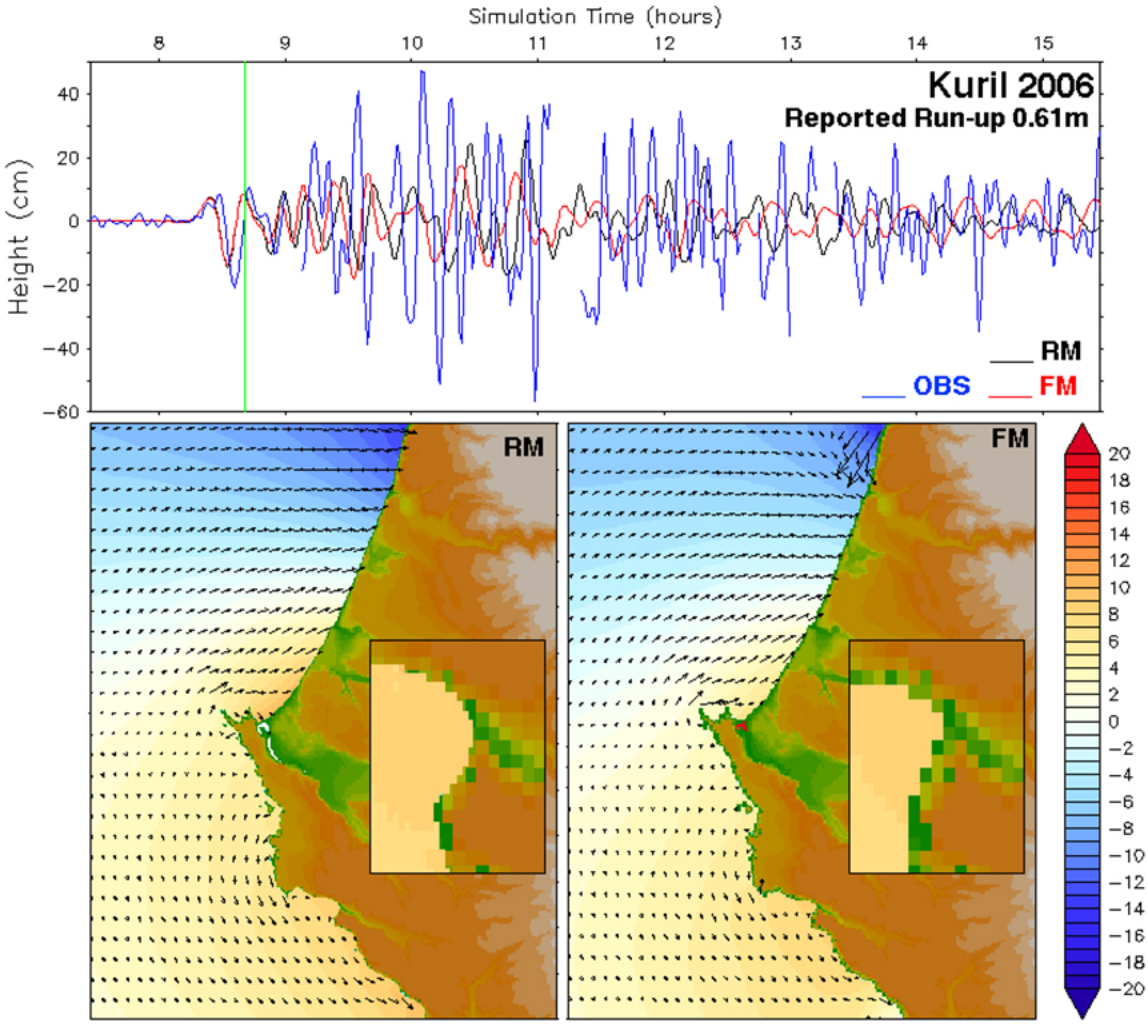

Figure 17. Comparison of RM and FM hind casts of the Kuril 2006 event to sea level fluctuations in Arena Cove, observed by the tsunami-capable tide gage.

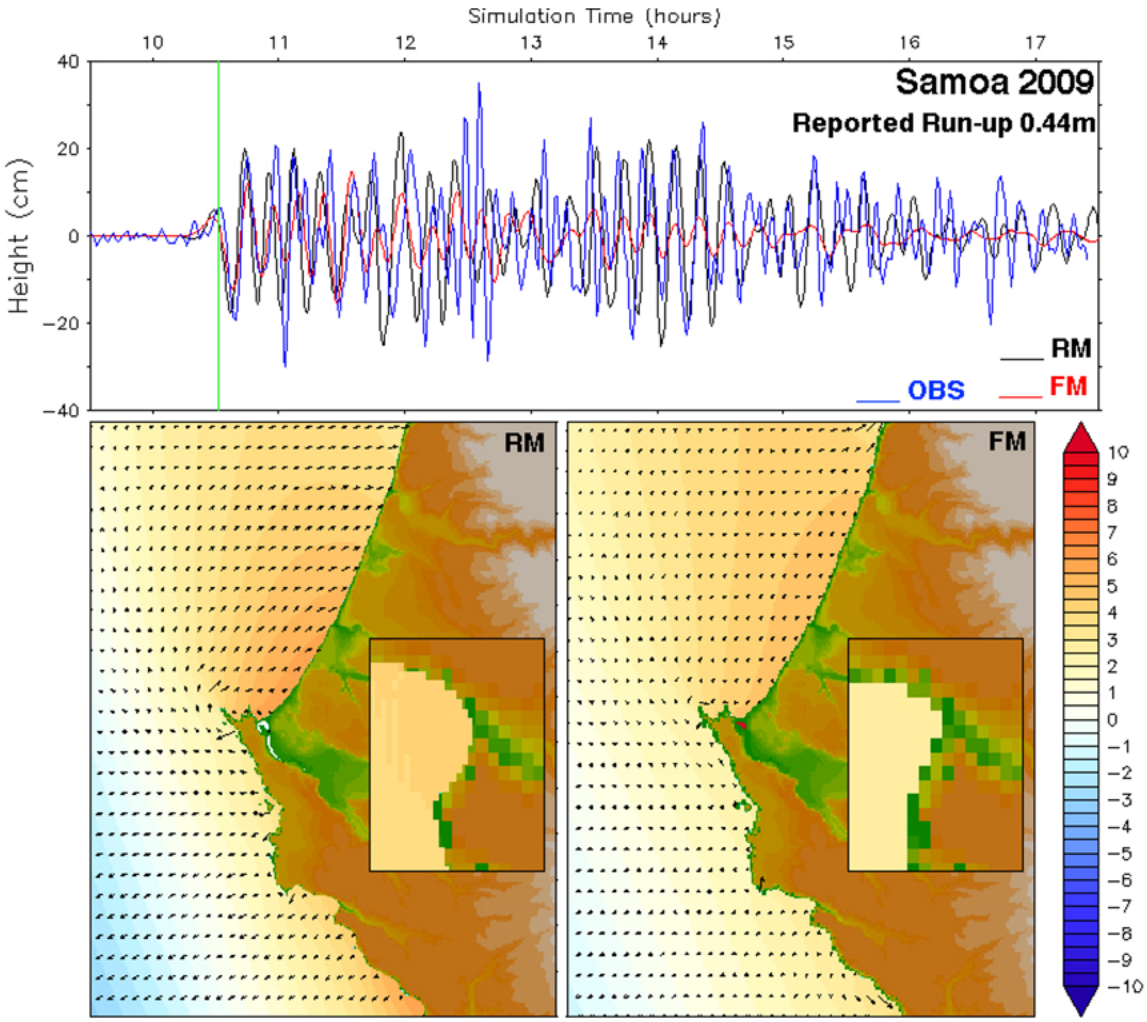

Figure 18. Comparison of RM and FM hind casts of the Samoa 2009 event to sea level fluctuations in Arena Cove.

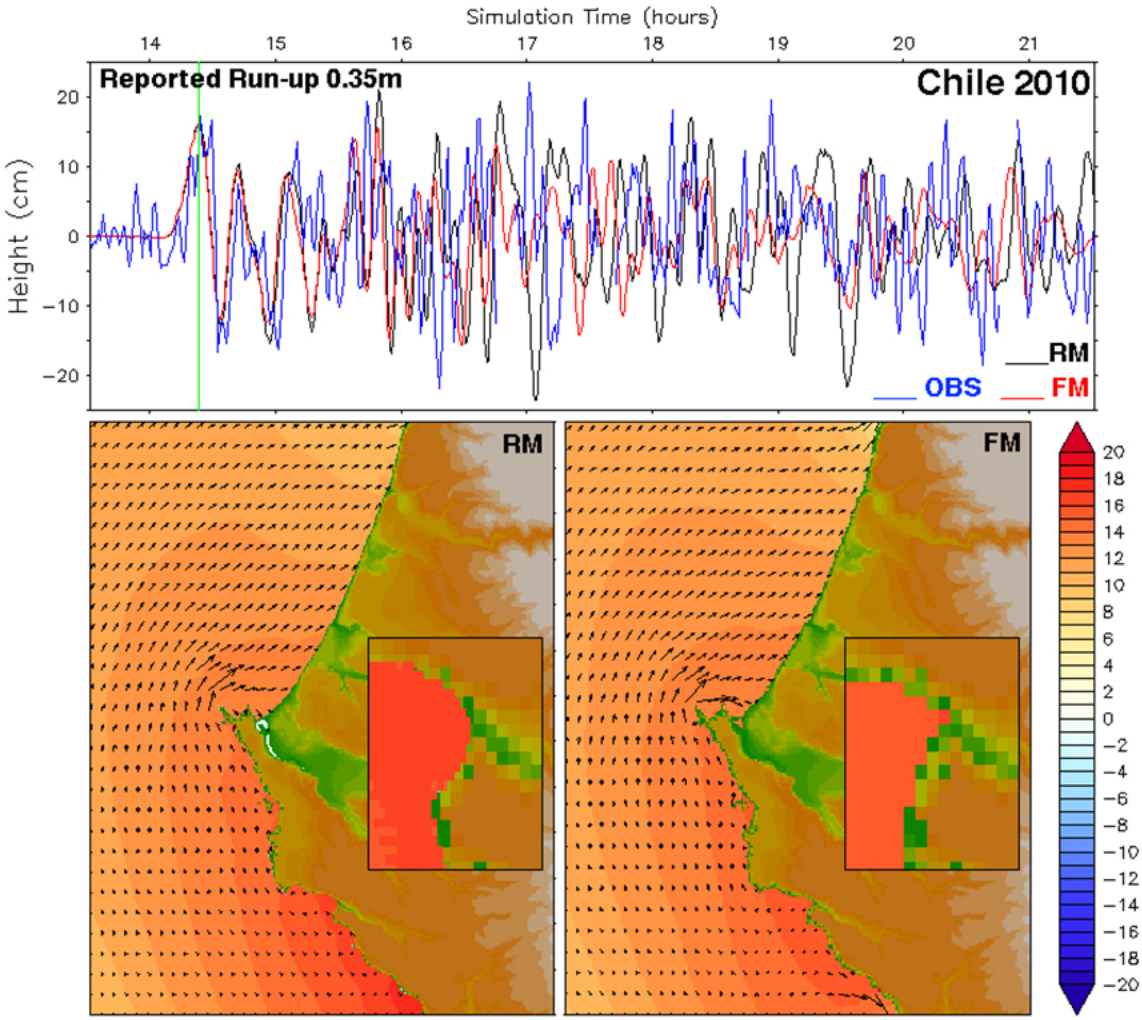

Figure 19. Comparison of RM and FM hind casts of the Chile 2010 event to sea level fluctuations in Arena Cove.

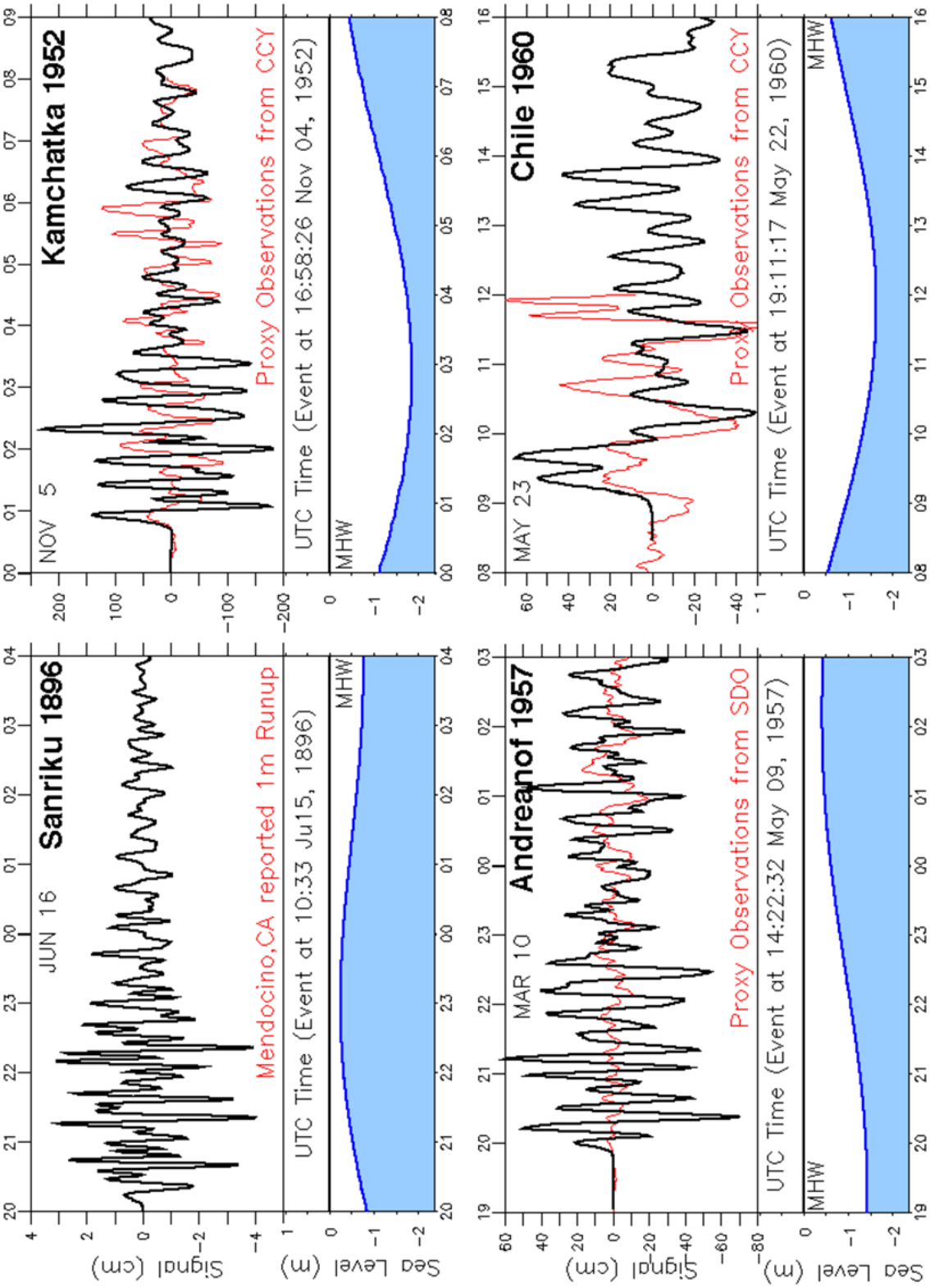

Figure 20. Simulated model response (FM) to the historical Sanriku 1896, Kamchatka 1952, Andreanof 1957 and Chile 1960 events. Proxy observations (in red) are provided where available from other California locations. The Sanriku 1896 result is not expected to match the observed run-up at nearby Mendocino. The state of the tide is shown and times are given as UTC.

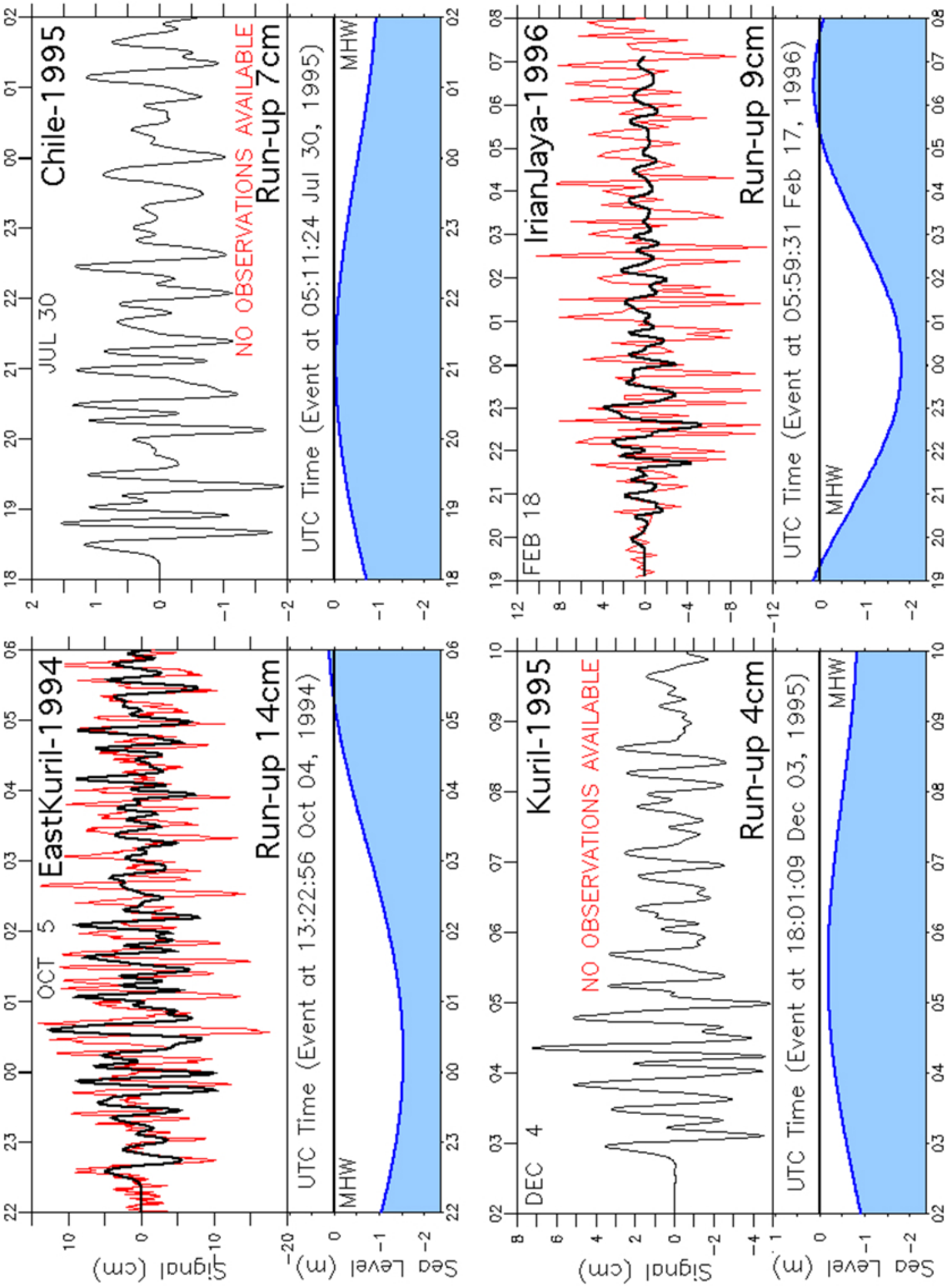

Figure 21. Model response (FM) to the East Kuril 1994, Chile 1995, Kuril 1995 and Irian Jaya 1996 events. Tide gage data (in red) where available is from Arena Cove.

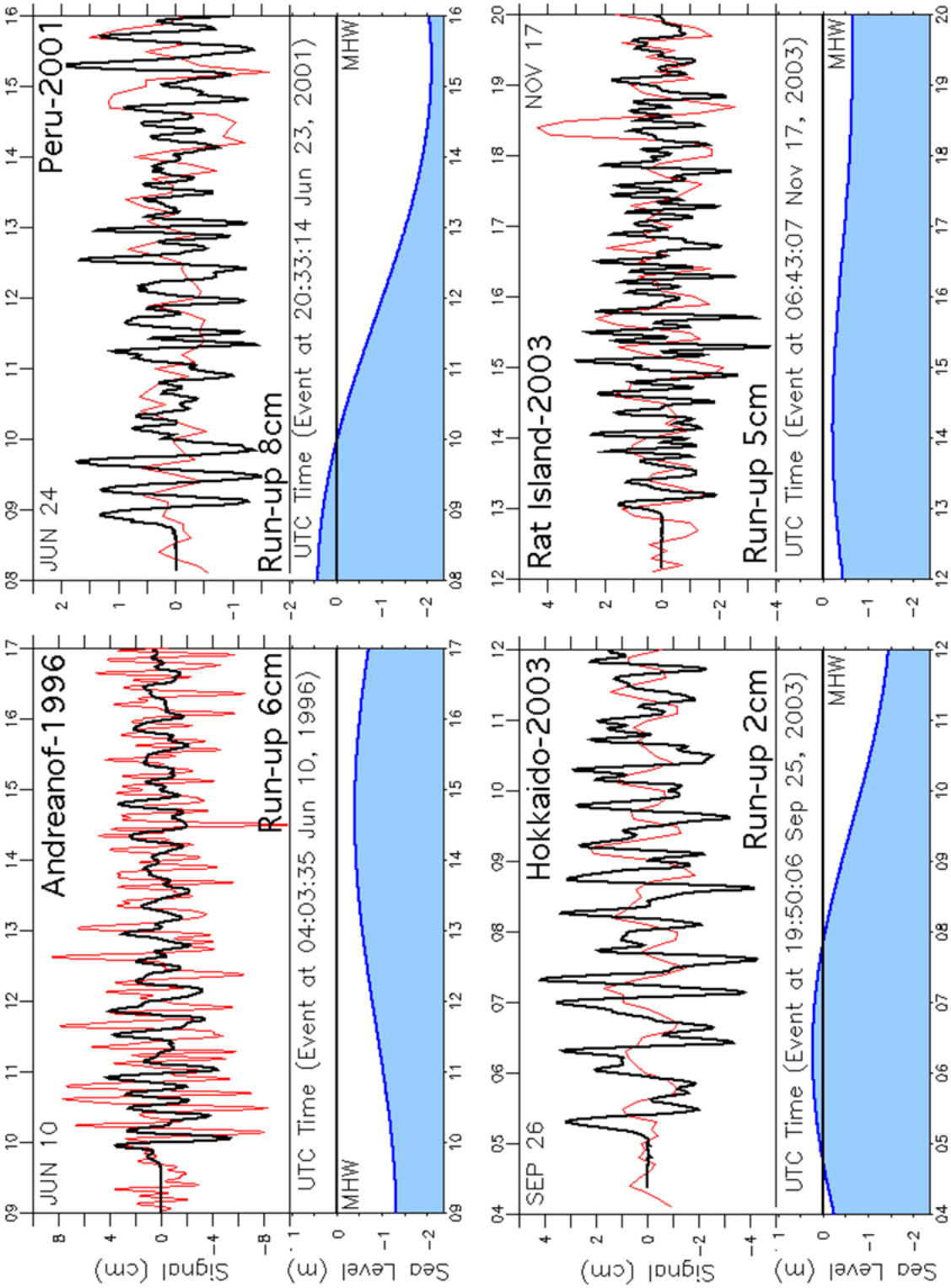

Figure 22. Model response (FM) to the Andreanof 1996, Peru 2001, Hokkaido 2003, and Rat Island 2003 events. Tide gage data (in red) are from Arena Cove.

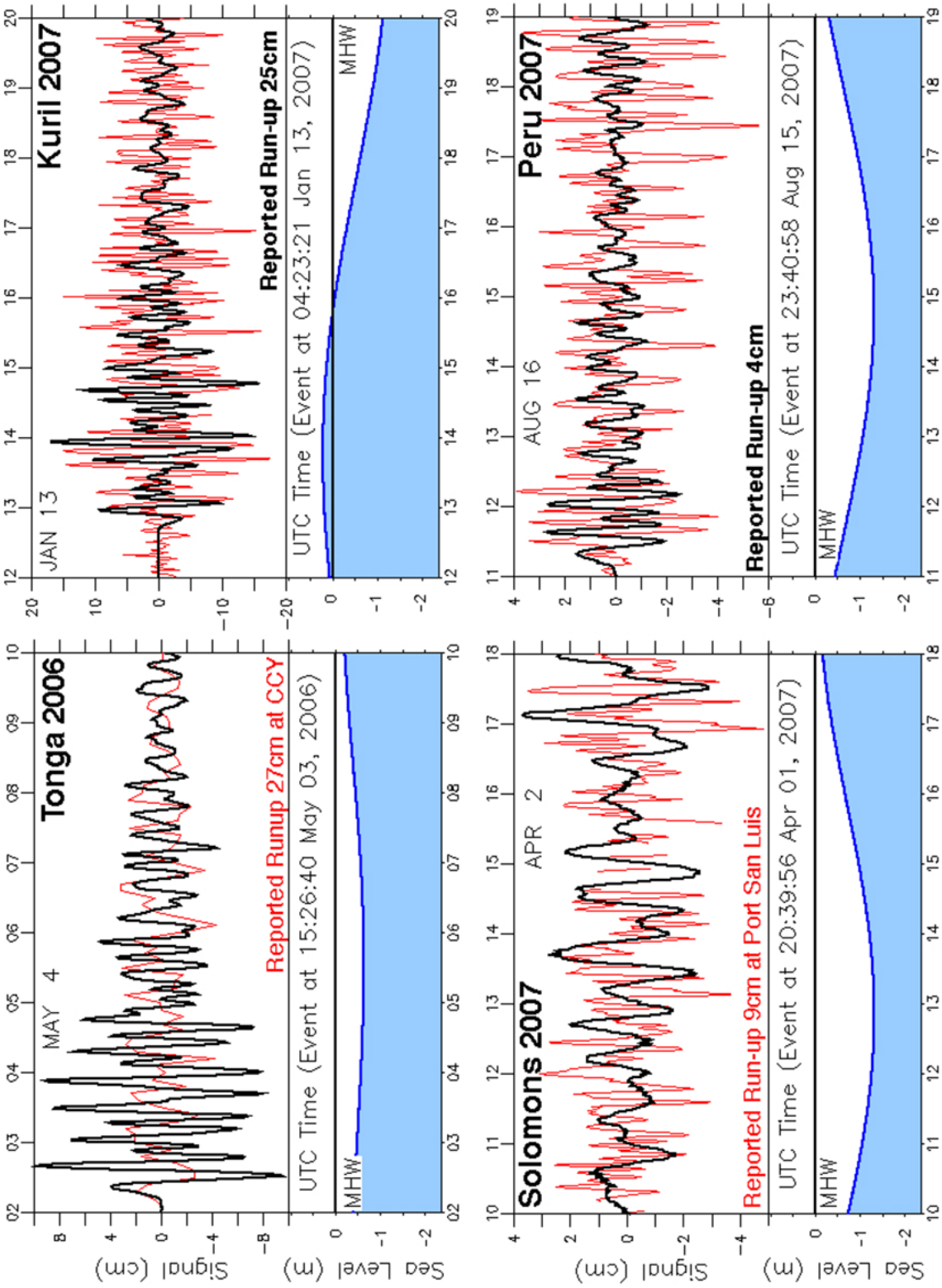

Figure 23. Model response (FM) to the Tonga 2006, Kuril 2007, Solomons 2007, and Peru 2007 events. Tide gage data (in red) are from Arena Cove

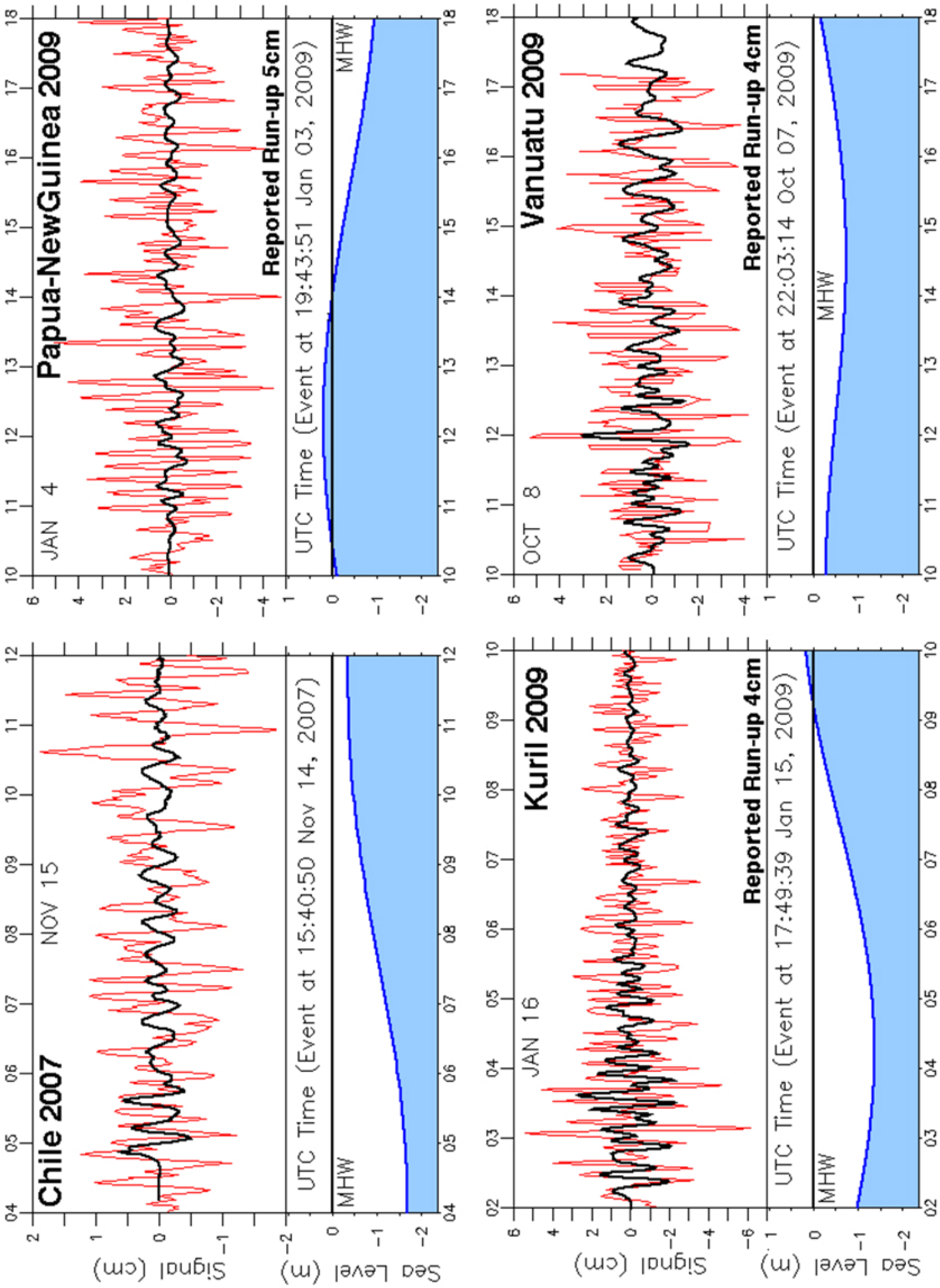

Figure 24. Model response (FM) to the Chile 2007, Papua-New Guinea 2009, Solomons 2009, and Vanuatu 2009 events. Tide gage data (in red) are from Arena Cove.

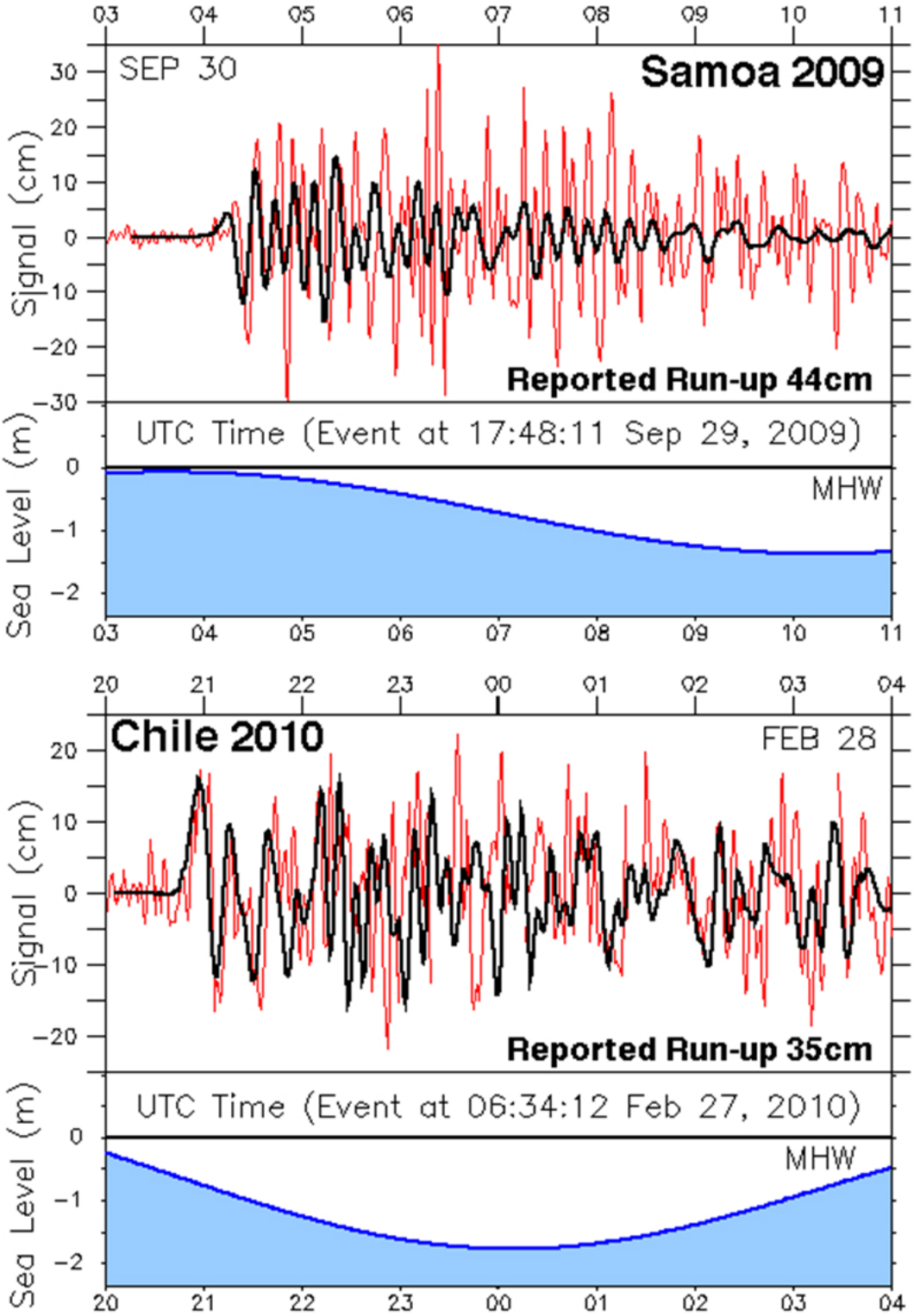

Figure 25. Model response (FM) to the Samoa 2009 and Chile 2010 events. Tide gage data (in red) are from Arena Cove.

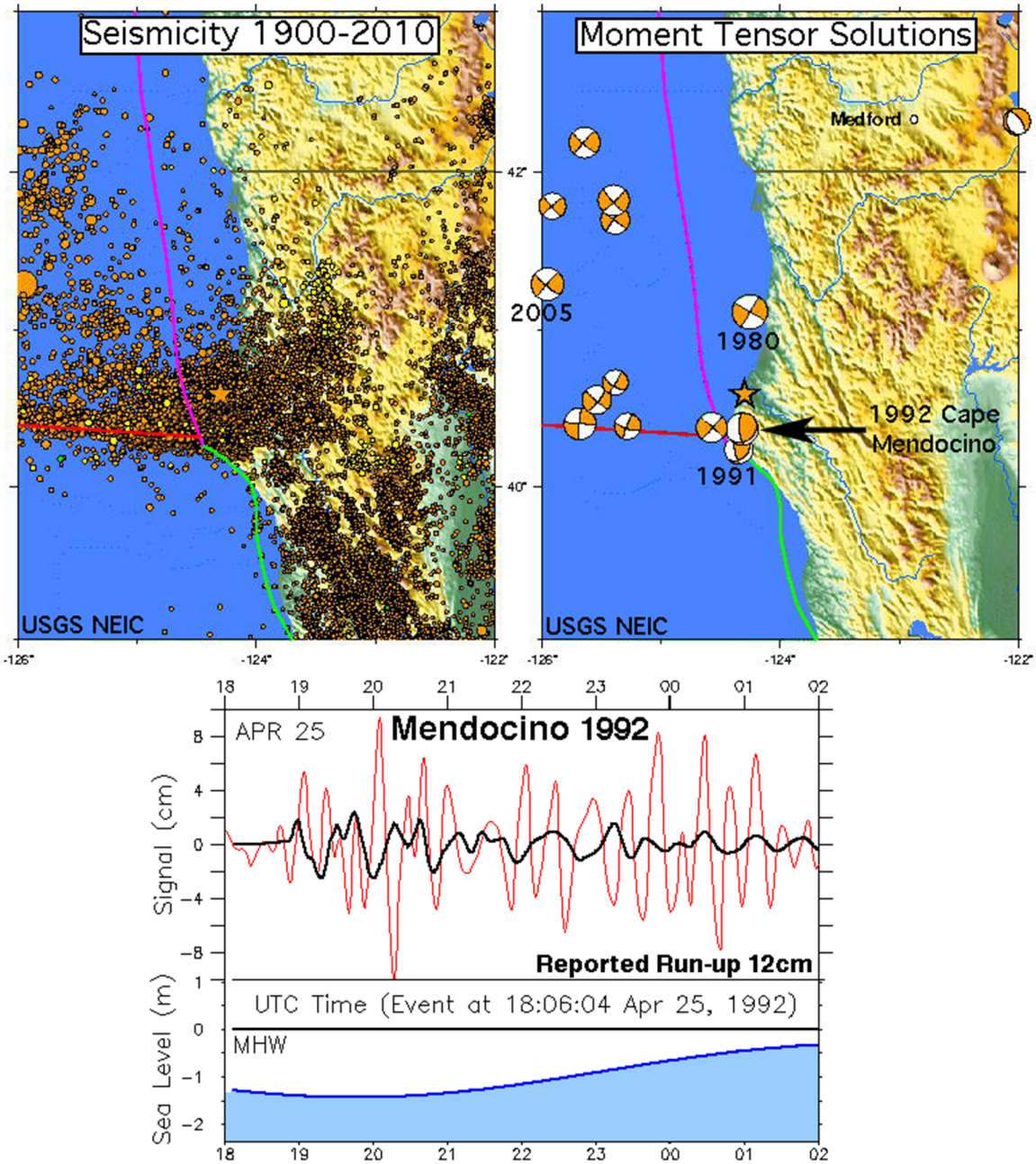

Figure 26. Seismicity in the vicinity of Cape Mendocino and the source mechanisms of notable recent earthquakes, adapted from USGC/NEIC products. The lower panel shows the poor agreement between the model and Arena Cove tide gage observations that is likely due to inadequate source representation in the model.

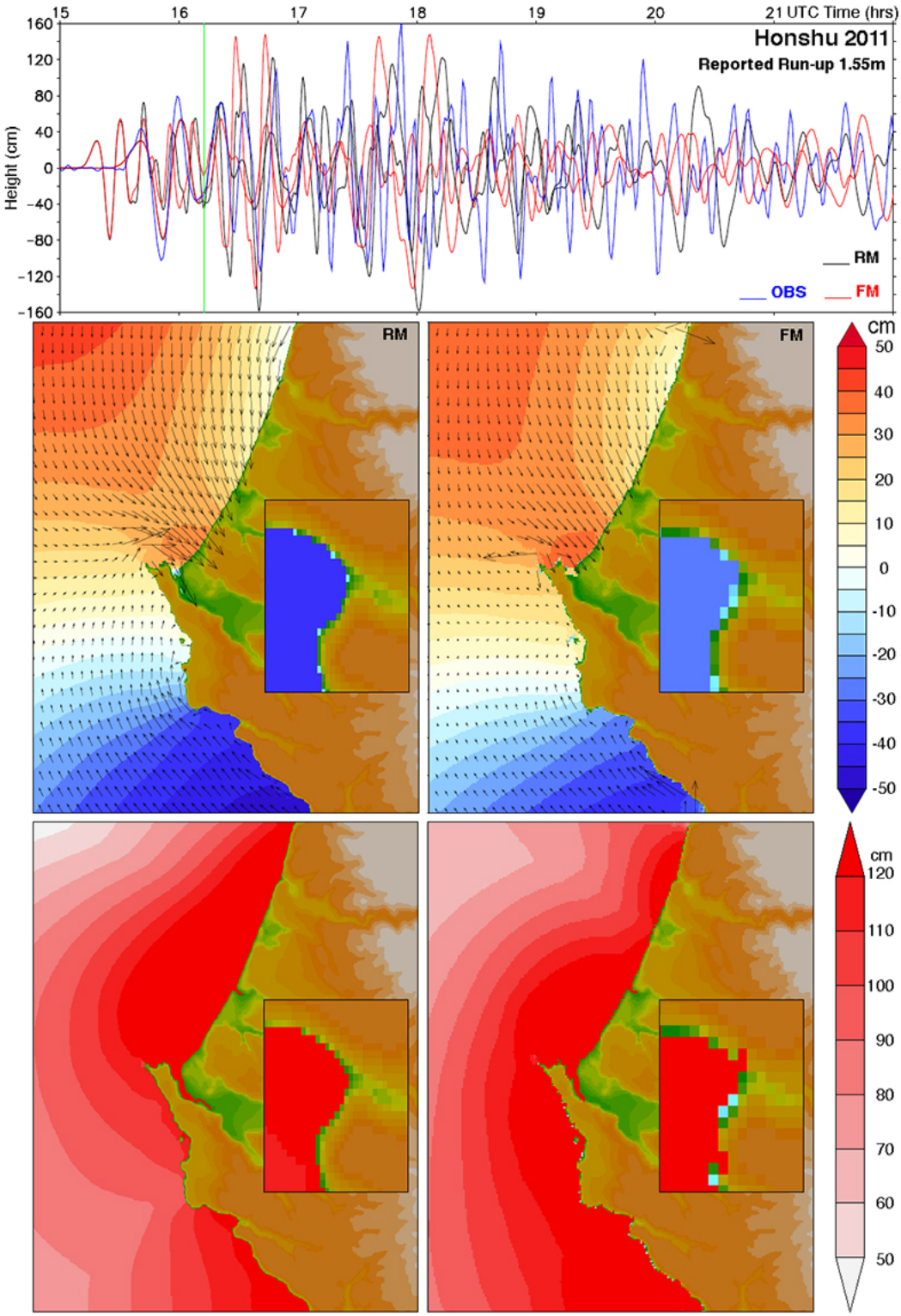

Figure 27. Comparison of FM real-time forecast and RM hindcast of the Honshu 2011 event with sea level observations in Arena Cove.

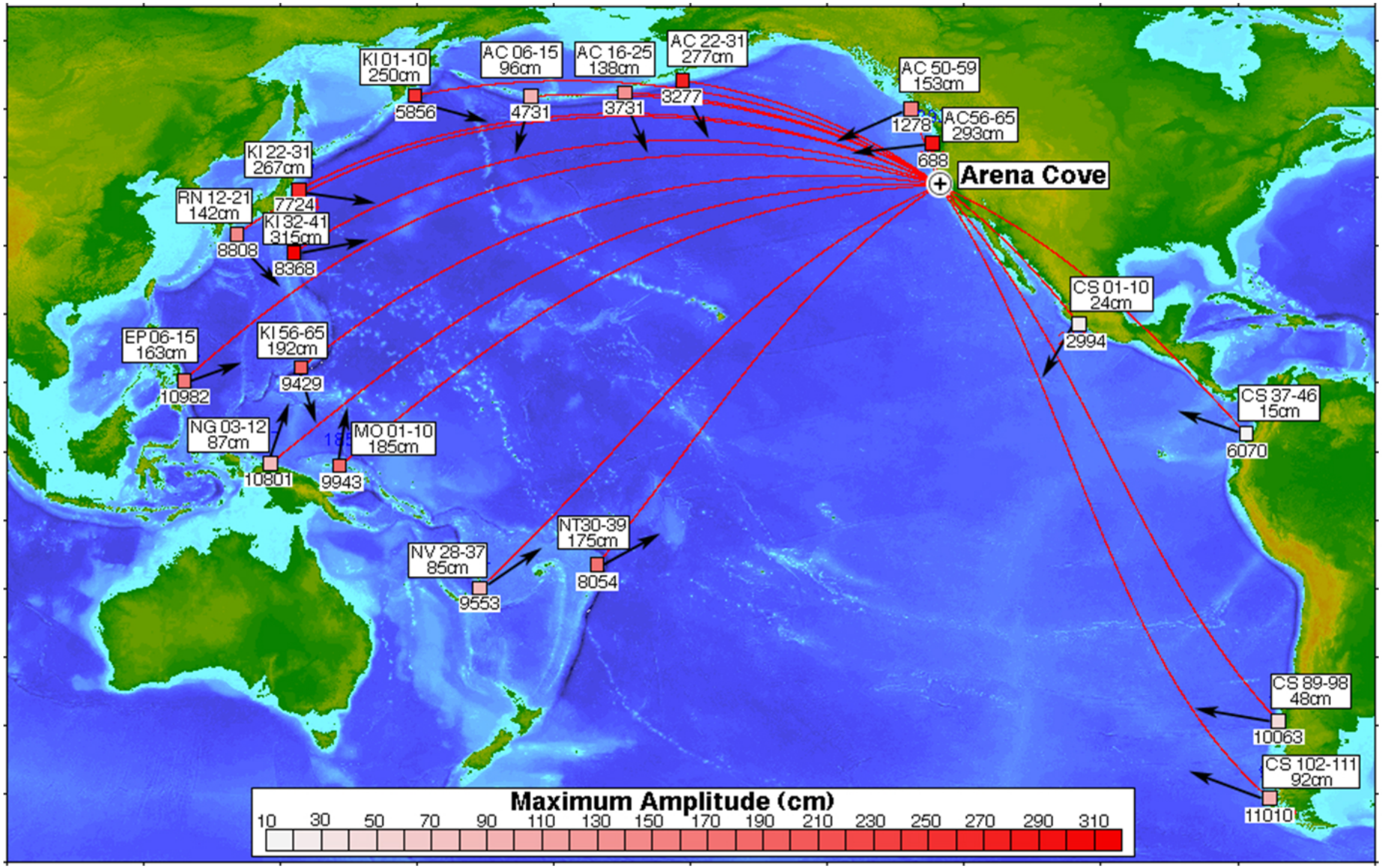

Figure 28. Predicted maximum sea level (from the FM) at the Arena Cove tide gage for the "mega-event" scenarios described in Table 6. Great circle routes are shown in red (with distances in km), and black arrows indicate the normal to the strike direction.

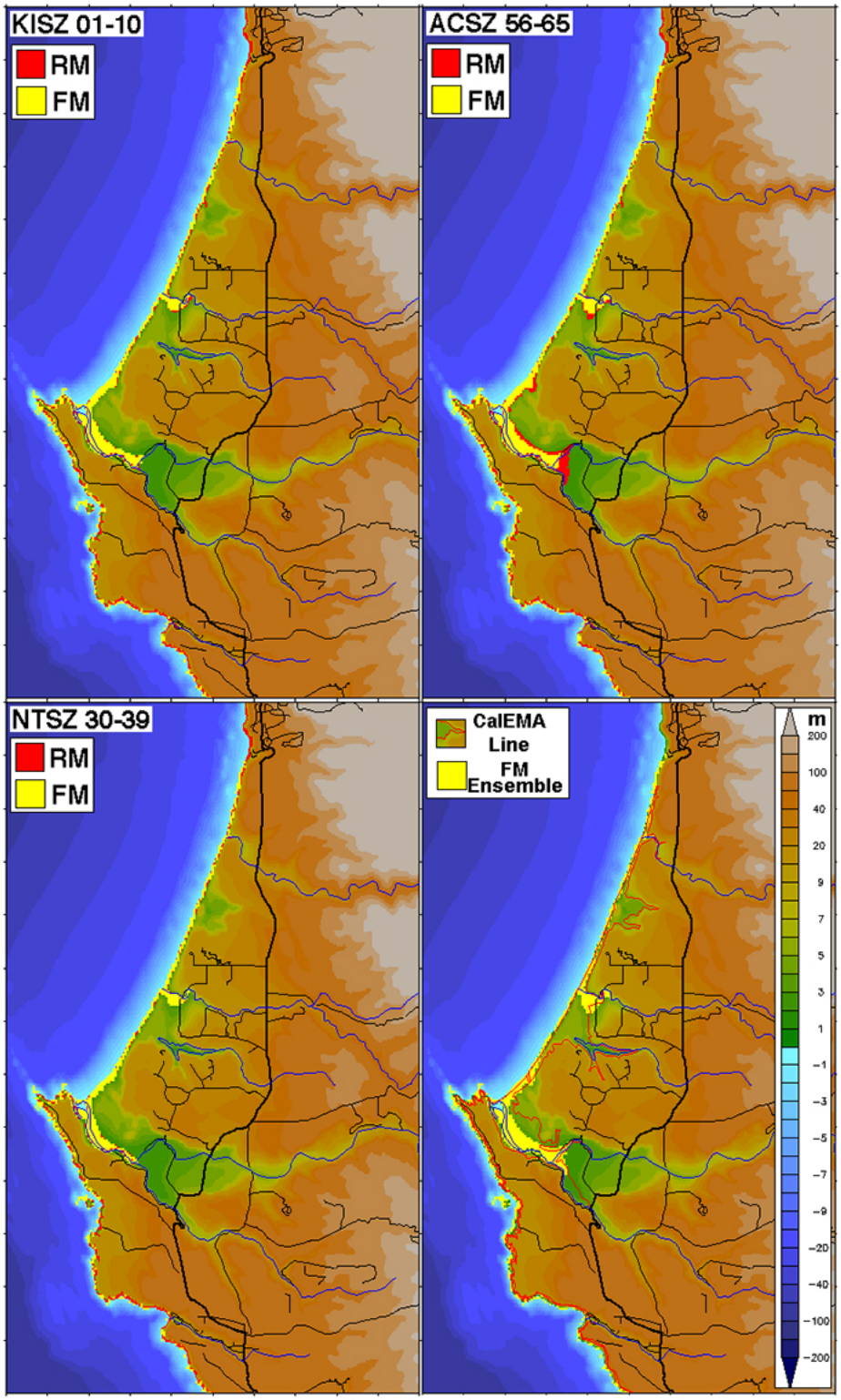

Figure 29. Comparison of RM and FM predictions for inundation of the Arena Cove / Manchester Beach region for selected mega-tsunami scenarios, and (lower right) for the ensemble employed in the CalEMA study.

Appendix A

A1. Reference Model Input (*.in) File for Arena Cove, CA

The following table contains the parameter and file choices used in the input file for the SIFT implementation (most3_facts_nc.in) of the reference model (RM) for Arena Cove, CA.

Parameter/File*	**Purpose**
0.0010	Minimum amp. of input offshore wave (m)
1.0	Minimum depth of offshore (m)
0.1	Dry land depth of inundation (m)
0.0009	Friction coefficient (n**2)
1	Let A-Grid and B-Grid run up
900.0	Max eta before blow-up (m)
0.6	Time step (sec)
48000	Total number of time steps in run
5	Time steps between A-Grid computations
1	Time steps between B-Grid computations
50	Time steps between output steps
0	Time steps before saving first output step
1	Save output every n-th grid point
ArenaCoveCA_RM_A.most	A-grid bathymetry file
ArenaCoveCA_RM_B.most	B-grid bathymetry file
ArenaCoveCA_RM_C.most	C-grid bathymetry file
./	Directory of source files
,/	Directory for output files

* The column headings are not part of most3_facts_nc.in

DRAFT

A2. Forecast Model Input (*.in) File for Arena Cove, CA

The following table contains the parameter and file choices used in the input file for the SIFT implementation (most3_facts_nc.in) of the optimized forecast model (FM) for Arena Cove, CA. When run on an Intel® Xeon® E5670 2.93GHz processor the model simulates four hours in 10.73 minutes, close to the 10-minute target for this metric.

Parameter/File*	**Purpose**
0.0010	Minimum amp. of input offshore wave (m)
1.0	Minimum depth of offshore (m)
0.1	Dry land depth of inundation (m)
0.0009	Friction coefficient (n**2)
1	Let A-Grid and B-Grid run up
900.0	Max eta before blow-up (m)
1.5	Time step (sec)
19200	Total number of time steps in run
4	Time steps between A-Grid computations
1	Time steps between B-Grid computations
20	Time steps between output steps
0	Time steps before saving first output step
1	Save output every n-th grid point
ArenaCoveCA_FM_A.most	A-grid bathymetry file
ArenaCoveCA_FM_B.most	B-grid bathymetry file
ArenaCoveCA_FM_C.most	C-grid bathymetry file
./	Directory of source files
,/	Directory for output files

* The column headings are not part of most3_facts_nc.in

DRAFT

Appendix B Propagation Database: Pacific Ocean Unit Sources

Appendix C Synthetic Testing Report

Glossary

DRAFT